Chaotic Phase-Coded Waveforms with Space-Time Complementary Coding for MIMO Radar Applications

Sheng Hong, Fuhui Zhou, *Member*, *IEEE*, Yantao Dong, Zhixin Zhao, Yuhao Wang, *Senior Member*, *IEEE*, Maosong Yan

***Abstract*—A framework for designing orthogonal chaotic phase-coded waveforms with space-time complementary coding (STCC) is proposed for multiple-input multiple-output (MIMO) radar applications. The phase-coded waveform set to be transmitted is generated with an arbitrary family size and an arbitrary code length by using chaotic sequences. Due to the properties of chaos, this chaotic waveform set has many advantages in performance, such as anti-interference and low probability of intercept. However, it cannot be directly exploited due to the high range sidelobes, mutual interferences, and Doppler intolerance. In order to widely implement it in practice, we optimize the chaotic phase-coded waveform set from two aspects. Firstly, the autocorrelation property of the waveform is improved by transmitting complementary chaotic phase-coded waveforms, and an adaptive clonal selection algorithm is utilized to optimize a pair of complementary chaotic phase-coded pulses. Secondly, the crosscorrelation among different waveforms is eliminated by implementing space-time coding into the complementary pulses. Moreover, to enhance the detection ability for moving targets in MIMO radars, a method of weighting different pulses by a null space vector is utilized at the receiver to compensate the interpulse Doppler phase shift and accumulate different pulses coherently. Simulation results demonstrate the efficiency of our proposed method.**

***Index Terms*—Multiple-input multiple-output radars, orthogonal waveforms, space-time complementary coding, Doppler compensation.**

I. Introduction

FOR multiple-input multiple-output (MIMO) radar applications, a set of transmitted waveforms with impulse-like autocorrelation and zero crosscorrelation can obtain a good detection performance [1], [2]. Recently, the chaotic sequences have been widely exploited in the waveform design for MIMO radars [5], [7] due to their inherent advantages in the randomness, no cycle, complexity, security, code generation speed, and the number of possible code sequences [3], [4]. A multicarrier chaotic phase-coded radar waveform was proposed in [8]. A new kind of frequency hopping codes based on chaotic sequences has been designed in [9], [10]. In [11], a chaotic waveform using wavelength-division multiplexing technology has been proposed for the distributed MIMO radar. By implementing the phase coding technique [12], [13] on chaotic sequences, a set of chaotic phase-coded waveforms was obtained [14], which is also a good waveform candidate for the MIMO radar detection. Due to the aperiodicity in chaotic dynamics, an impulse-like autocorrelation function of the chaotic phase-coded waveform can be approached. Due to the sensitivity of chaotic systems to the initial values, the quasi-orthogonality among different chaotic phase-coded waveforms can be achieved. Furthermore, the chaotic phase-coded waveforms with an arbitrary family size, code length, and phase number can be easily generated, and they also well match with the requirements of anti-jamming and low probability of intercept (LPI) for modern radars. However, the primary chaotic phase-coded waveforms cannot be used directly for the MIMO radar detection due to high range sidelobe level, large mutual interference, and Doppler intolerance. In order to tackle these problems, further waveform optimization and signal processing are proposed based on the primary chaotic phase-coded waveforms.

To suppress the high range sidelobes and reduce the mutual interferences in the MIMO radar waveform set, in general, there exist two research strategies for waveform design. The first strategy is to jointly optimize the autocorrelation and crosscorrelation properties of the waveform set. Many statistical optimization algorithms, such as the simulated annealing algorithm [15], cross entropy-based [16] methods, genetic algorithm [17], particle swarm algorithm [18], and iterated algorithm [19], [20] were proposed to design a set of orthogonal unimodular sequences, which are then modulated by phase-coding on a long transmitted pulse. For these optimization algorithms, the family size and code length of the optimized waveform set are very limited due to the heavy computational load, large calculation storage, and high time cost. The second strategy is to separately optimize the autocorrelation and crosscorrelation properties of the waveform set. In this strategy, many traditional radar waveforms with good aperiodic autocorrelation properties can be borrowed into the MIMO radar with orthogonal division multiplexing techniques for achieving the waveform orthogonality. The traditional radar waveforms employed in real radar systems mainly consist of the LFM

Sheng Hong is with the School of Information Engineering, Nanchang University, P. R. China, 330031, and she is also with Postdoctoral Research Station of Mechanical Engineering, Nanchang University, P. R. China, 330031. (email: shenghong@ncu.edu.cn). Fuhui Zhou is with the Department of Electrical and Computer Engineering at Utah State University, Logan, UT 84322 USA (e-mail: zhoufuhui@ieee.org). Yantao Dong, Zhixin Zhao, Yuhao Wang, and Maosong Yan are with the School of Information Engineering. (e-mail: 406130717274@email.ncu.edu.cn, zhaozhixin@ncu.edu.cn, wangyuhao@ncu.edu.cn, 406130715100@email.ncu.edu.cn).

This work was supported by the National Natural Science Foundation of China (61661032, 61461030, 61761030), the Young Natural Science Foundation of Jiangxi Province (20161BAB212038), the Young Science and Technology Research Foundation of Jiangxi Province (GJJ150097), and the China Postdoctoral Science Foundation (2017M622102, 2017M622103).

waveforms and phase-coded waveforms [21], [22], [14]. The phase-coded waveforms are preferred due to their almost ideal aperiodic autocorrelation properties and easy generation. The complementary phase-coded waveform is a special kind of phase-coded waveforms which have an ideal autocorrelation property (i.e. strictly impulse-like aperiodic autocorrelation function) by modulating the complementary phase-coded sequences on consecutive transmitted pulses [24], [25]. Since the ideal autocorrelation property cannot be achieved with a single phase-coded sequence, we exploit the complementary phase-coded sequences from the traditional radar into the MIMO radar in this paper. To obtain the orthogonality among different waveforms in the MIMO radar, the orthogonal time/frequency/code division multiplexing techniques are usually exploited. The time division technique was utilized in the MIMO-OTHR [26] to construct a kind of "time-staggered" linear frequency-modulated (LFM) continuous waveforms, and the drawback is that only one signal can be transmitted at an instant of time. The frequency division technique was exploited in a kind of LFM waveforms modulated on different frequencies for the MIMO radar detection [27], but the cost is the requirement of a large bandwidth. The typical method to reduce the crosscorrelation by the code division is the space-time coding [28], which is relatively superior to the other two division techniques without extra frequency spectrum and time resources [29]. Moreover, the code division technique can mitigate the decrease of the coherence of targets in the time division and frequency division techniques. Therefore, the achievement of a good orthogonality with code division is preferred in many theoretical analysis and practical MIMO radar systems. In this paper, we employ the second strategy to flexibly design chaotic phase-coded waveforms in a simple and quick way. The architecture of complementary sequences is optimized to achieve low sidelobes of the autocorrelation function, and the space-time coding is utilized to achieve the orthogonality.

The phase-coded waveforms are usually Doppler intolerant [30]. The solutions of this problem can be classified into two categories. The first category is to consider the correlation properties for all possible Doppler frequencies in the cost function of the waveform optimization, which is implemented at the transmitter. Essentially, it is to optimize the auto-ambiguity function and the cross-ambiguity function of the waveforms. However, the optimization process is extremely clumsy even for a small set of short sequences [20], [31], [32], [33], [15]. For complementary waveforms, the low-order terms of the Taylor expansion of the pulse train ambiguity function were derived, and then the Doppler resilient Golay complementary sequences were designed [34], [35]. However, the designed complementary sequences are still stringently limited by the number and length of the sequences, and they are only tolerant at modest Doppler shifts. The other category is to compensate the Doppler shifts through signal processing methods at the receiver [36]. The typical approach is to use a bank of Doppler-matched filters [37]. In this paper, we utilize the second category to obtain the Doppler resilience of our designed chaotic phase-coded waveforms. The challenge is that the Doppler phase shifts over several pulses instead of a single pulse have to be compensated.

By thoroughly addressing those three issues of autocorrelation, crosscorrelation, and Doppler resilience, the chaotic phase-coded waveforms with space-time complementary coding (STCC) are well-designed. The overall designing process can be divided into four steps. Firstly, the chaotic phase-coded sequences are mapped from the discrete chaotic sequences, and modulated on the transmitted pulse. The resultant waveforms are identified as the primary chaotic phase-coded waveforms. It means that the waveforms are constructed by the chaotic sequences solely. Secondly, the approximately complementary chaotic phase-coded sequences are optimized by a properly-selected optimization algorithm. Specifically, a chaotic sequence is randomly-generated. Then, an adaptive clonal selection (ACS) algorithm [38] is introduced to optimize its complementary partner. By transmitting a pair of complementary chaotic phase-coded waveforms, the sidelobes of the autocorrelation function can be greatly reduced. This process is sensitive to the initial value. Thus, if the process is repeated independently by M times, M independent pairs of complementary chaotic phase-coded waveforms are obtained, and they are quasi-orthogonal. Thirdly, the space-time coding is further implemented on the complementary chaotic phase-coded waveforms to completely eliminate the crosscorrelation among different transmitted waveforms. This kind of waveforms are identified as the chaotic phase-coded waveforms with STCC. Finally, a method of weighting multiple received pulses by a null-space vector is utilized to compensate the Doppler shift and accumulate different pulses coherently at the receiver. This manipulation can significantly enhance the Doppler tolerance of the chaotic phase-coded waveforms with STCC.

Although the thought of Golay complementary codes with STCC has been studied in [39], [50], the length and number of the codes are fixed. In this paper, the optimized complementary chaotic sequences are exploited in the STCC, and the Doppler resilience of the STCC is obtained, which is more feasible in practical applications. The main contributions of this paper are summarized as follows.

1) Multiple chaotic phase-coded pulses are designed by implementing the STCC on the primary chaotic phase-coded waveforms for achieving the required autocorrelation and crosscorrelation properties. The Doppler tolerance of the designed waveforms is achieved by utilizing a Doppler compensation method at the receiver. Compared with the traditional waveform optimization for MIMO radars, our design process is simpler, and the waveform performance is superior.
2) To optimize the complementary chaotic sequences, a non-linear optimization problem is formulated, and an adaptive clonal selection algorithm is proposed to solve it. Generally, the number, length, and phase number of the existing strictly-complementary sequences are stringently limited, and our optimization on the complementary architecture can break this limitation to enable the wide application of complementary sequences. Moreover, if the process is repeated independently, a degree of orthogonality between different pairs of complementary

chaotic sequences can be obtained. Thus, they can be utilized for MIMO radar detection in the cases that the orthogonality is not highly required.

3) Simulation results demonstrate that the chaotic phase-coded waveforms with STCC are relatively more sensitive to the Doppler frequency compared with the typical orthogonal phase-coded waveforms (e.g., the Deng's phase-coded waveforms). The main reason is that the STCC is Doppler-intolerant. In this sense, the utilized Doppler compensation method is benefit to solve the Doppler intolerance of the STCC.

The rest of this paper is organized as follows. In Section II, the concise signal model, MIMO ambiguity function, synthetic output of the primary chaotic phase-coded waveforms in the MIMO radar are derived. The sophisticated waveform design approach is proposed in Section III. In Section IV, simulation results are presented. Finally, Section V concludes the paper.

II. Signal Model in the MIMO Radar

A. Phase-Coded Waveforms for the MIMO Radar

Without loss of generality, it is assumed that M_t waveforms denoted by $\boldsymbol{S} = [s_1(t), s_2(t), \cdots, s_{M_t}(t)]^T$ are emitted from M_t transmitting antennas. $s_m(t)$ is the phase-coded waveform modulated on the carrier frequency f_0 transmitted by the mth antenna. To obtain a good Doppler resolution, a coherent train of pulses is transmitted. The train can be constructed from identical pulses or identical pair/set of different pulses. We consider the later case in this paper. For the sake of easy explantation, a pair of different phase-coded pulses are assumed to be modulated on $s_m(t)$ and repeatedly transmitted in succession. Then, $s_m(t)$ can be expressed as

$$s_m(t) = (A_m(t) + B_m(t - T_r))\exp(j2\pi f_0 t) \tag{1}$$

$$A_m(t) = \sum_{l=0}^{L-1} \exp(ja_m(l))u(t - lT_s) \tag{2}$$

$$B_m(t) = \sum_{l=0}^{L-1} \exp(jb_m(l))u(t - lT_s) \tag{3}$$

$$u(t) = \begin{cases} 1, & \text{if} \quad 0 < t < T_s \\ 0, & \text{otherwise} \end{cases} \tag{4}$$

$$a_m(l), b_m(l) \in \left\{ 0, \frac{2\pi}{M_c}, 2\frac{2\pi}{M_c}, \cdots, (M_c - 1)\frac{2\pi}{M_c} \right\} \tag{5}$$

where $m = 1, 2, \cdots, M_t$. $A_m(t)$ and $B_m(t)$ are the complex envelopes of the two consecutive phase-coded pulses modulated on $s_m(t)$. $u(t)$ is the rectangular window of duration T_s with unit amplitude for symbol modulation. $a_m(l)$ and $b_m(l)$ are the lth code symbols mapped on the mth subcarrier, and M_c is the phase number. The $\boldsymbol{a}_m = [a_m(0), a_m(1), \cdots, a_m(L-1)]^T$ and $\boldsymbol{b}_m = [b_m(0), b_m(1), \cdots, b_m(L-1)]^T$ are defined as the phase-coded sequences corresponding to $A_m(t)$ and $B_m(t)$. The code length is L, and T_s is the sub-pulse width. Thus $T_p = LT_s$ denotes the time width of a single pulse. T_r is the pulse repetition interval (PRI).

B. Chaotic Phase-Coded Waveforms

Compared with the traditional pseudo random sequences, chaotic sequences have the advantages in the large number, sensitivity, long length, aperiodicity, and easy generation. Chaotic phase-coded waveforms generated from chaotic sequences inherit these advantages, thus are suitable for MIMO radar detection. The randomness and security of coded waveforms are guaranteed, and the requirements for the code number and length can be satisfied easily. The discrete chaotic sequence is generated according to the chaotic map. Typical chaotic maps include the bernoulli, logistic, tent, quadratic maps, and so on. These chaotic maps generate the commonly-used one-dimensional chaotic sequences, and the specific map functions can be referred to [40]. Based on them, more complex chaotic sequences are proposed. A hybrid logistic-tent map was constructed in [41] to produce spread spectrum sequences. Reference [42] proposed a hyper logistic phase-coded waveform for radar applications.

The discrete chaotic sequence is generally mapped into the phase-coded sequence [43] by using the threshold quantization method. Assume that the chaotic sequence is $x_m(l), l = 0, 1, 2, \cdots, L-1$, then $x_m(l)$ can be generated by a non-linear chaotic map function $\Phi(\cdot)$, given as

$$x_m(l+1) = \Phi(x_m(l)) \tag{6}$$

where the chaotic sequences are normalized into $x_m(l) \in (0, 1)$. Then $x_m(l)$ is quantized and mapped into phase-coded sequence $a_m(l)$ (or $b_m(l)$). The specific steps are described as follows.

1) Set an arbitrary initial value $x_m(0)$, and $x_m(0) \in (0, 1)$.
2) Generate the chaotic sequence $\{x_m(l^\circ)\}$, $1 \le l^\circ \le L + 999$ according to the chaotic map in (6). In order to reduce the influence of the initial value, the first 1000 points are removed to improve the complexity of the chaotic sequence. Then a chaotic sequence $\{x_m(l)\}$, $l = 0, 1, \cdots, L-1$ is obtained.
3) Quantize the chaotic sequences $\{x_m(l)\}$ into M_c phases according to their values in different intervals divided by $M_c - 1$ thresholds. These thresholds divide the range $[0, 1]$ evenly. Then the chaotic phase-coded sequence $\{a_m(l)\}$ is mapped from $\{x_m(l)\}$ by $a_m(l)$=2πceil$(M_c x_m(l) - 1)/M_c$.

By repeating these steps independently by M_t times, M_t chaotic phase-coded sequences $\{a_m(l)\}_{l=0,1,\cdots L-1}$, $m = 1, 2, \cdots M_t$ can be obtained. These M_t sequences are approximately independent of each other due to the independent and random initial values for the chaotic map. We identify these directly-mapped phase-coded sequences as the primary chaotic phase-coded sequences. If the period L is infinitely long and the numerical precision is infinitely high, the autocorrelation function of the primary chaotic phase-coded sequence is an ideal Dirac delta function, and the crosscorrelation between different sequences is zero. In practical situations, only the chaotic sequences with a finite length are utilized. Thus the ideal autocorrelation property and orthogonality can only be approached approximately. Actually, the range sidelobes of primary chaotic phase-coded sequences are still very high, and

This article has been accepted for publication in a future issue of this journal, but has not been fully edited. Content may change prior to final publication. Citation information: DOI 10.1109/ACCESS.2018.2859404, IEEE Access

the mutual interferences are severe. It is essential to further optimize the chaotic phase-coded sequences for obtaining a better detection performance in MIMO radars.

C. The Synthetic Output and MIMO Ambiguity Function

In MIMO radar systems, a bank of matched filters corresponding to different transmitted waveforms are utilized at the receiver to detect targets. For M_t transmitted waveforms, there are M_t matched filters corresponding to the waveforms $s_1(t), s_2(t), \cdots, s_{M_t}(t)$ respectively. Assume that the target's delay is zero and that the target's Doppler frequency is f_d. Then the total received signal can be written as $x(t) = [s_1(t) + s_2(t) + \cdots + s_{M_t}(t)]\exp(j2\pi f_d t)$, where the spatial delay of the transmitting array is ignored for convenience. When $x(t)$ is matched filtering corresponding to $s_m(t)$, the filtered output can be represented as

$$\begin{aligned} R_{rm}(s_m, \boldsymbol{S}, f_d) &= \int_{-\infty}^{+\infty} x(t)s_m^*(t+\tau)dt \\ &= \int_{-\infty}^{+\infty} s_m(t)s_m^*(t+\tau)\exp(j2\pi f_d t)dt \\ &+ \sum_{n\neq m, n=1}^{M_t} \int_{-\infty}^{+\infty} s_n(t)s_m^*(t+\tau)\exp(j2\pi f_d t)dt \\ &\triangleq \chi_{s_m}(\tau, f_d) + \sum_{n\neq m, n=1}^{M_t} \chi_{s_m,s_n}(\tau, f_d) \end{aligned} \tag{7}$$

where $\chi_{s_m}(\tau, f_d)$ is just the auto-ambiguity function (auto-AF) of s_m, and $\chi_{s_m,s_n}(\tau, f_d)$ is just the cross-ambiguity function (cross-AF) between s_m and s_n. To evaluate the overall performance of the pulse compression results of the M_t matched filters, a synthetic filtered output is defined as

$$\begin{aligned} R_r(\boldsymbol{S}, f_d) &\triangleq \sum_{m=1}^{M_t} |R_{rm}(s_m, \boldsymbol{S}, f_d)| \\ &= \sum_{m=1}^{M_t} \left| \chi_{s_m}(\tau, f_d) + \sum_{n\neq m, n=1}^{M_t} \chi_{s_m,s_n}(\tau, f_d) \right| \\ &\triangleq \chi(\tau, f_d). \end{aligned} \tag{8}$$

According to the classic definition of MIMO ambiguity function (MIMO-AF) [44], it is found from (8) that the defined synthetic output is equivalent to the MIMO-AF. The ambiguity function (AF) is usually employed in radar for evaluating the waveform performance of target detection, target resolution, target estimation, and so on. In this paper, we mainly consider the target detection ability of the waveforms in MIMO radar. Since the target is detected from the synthetic output of the M_t matched filters, we take the synthetic output as the indicator to evaluate the waveform performance.

To optimize the synthetic output of the waveforms, the equation of $R_r(\boldsymbol{S}, f_d)$ is further derived from the expansion of the MIMO-AF $\chi(\tau, f_d)$. The $\chi(\tau, f_d)$ is composed of $\chi_{s_m}(\tau, f_d)$ and $\chi_{s_m,s_n}(\tau, f_d)$. If the transmitted signal $s_m(t)$ is sampled into the discrete signal $s_m(lT_s), l = 0, 1, \cdots, (L-1)$, the auto-ambiguity function $\chi_{s_m}(kT_s, f_d)$ can be written as

$$\begin{aligned} \chi_{s_m}(kT_s, f_d) =& \chi_u(0, f_d)[\chi_{a_m}(kT_s, f_d) \\ &+ \exp(j2\pi f_d T_r)\chi_{b_m}(kT_s, f_d)] \end{aligned} \tag{9}$$

where $k = -(L-1), \cdots, 0, \cdots, (L-1)$ and

$$\chi_u(0, f_d) = \frac{\exp(j\pi f_d T_s)\sin(\pi f_d T_s)}{\pi f_d T_s} \tag{10}$$

$$\chi_{a_m}(kT_s, f_d) = \sum_{l=0}^{L-|k|-1} \frac{[\exp(ja_m(l))][\exp(ja_m(l+|k|))]^*}{\exp(j2\pi f_d l T_s)}. \tag{11}$$

The $\chi_{b_m}(kT_s, f_d)$ can be directly obtained by replacing the code sequence $\boldsymbol{a}_m$ in (11) by $\boldsymbol{b}_m$. The detail derivations can be referred in Appendix A.

Similarly, the cross-ambiguity function $\chi_{s_m,s_n}(kT_s, f_d)$ can be written as

$$\begin{aligned} \chi_{s_m,s_n}(kT_s, f_d) =& \chi_u(0, f_d)[\chi_{a_m,a_n}(kT_s, f_d) \\ &+ \exp(j2\pi f_d T_r)\chi_{b_m,b_n}(kT_s, f_d)] \end{aligned} \tag{12}$$

where $k = -(L-1), \cdots, 0, \cdots, (L-1)$ and

$$\chi_{a_m,a_n}(kT_s, f_d) = \sum_{l=0}^{L-|k|-1} \frac{[\exp(ja_n(l))][\exp(ja_m(l+|k|))]^*}{\exp(j2\pi f_d l T_s)}. \tag{13}$$

The $\chi_{b_m,b_n}(kT_s, f_d)$ can be directly obtained by replacing the code sequence $\boldsymbol{a}_m$ in (13) by $\boldsymbol{b}_m$. The detail derivations can be referred in Appendix B.

By substituting (9) and (12) into (8), the synthetic output $R_r(\boldsymbol{S}, k, f_d)$ can be obtained. Generally, the performance of the synthetic output is indicated by its sidelobe level. The sidelobe level should be low to reduce the false alarm probability. In most cases, the peak sidelobe level (PSL) and the integrated sidelobe level (ISL) of the synthetic output are utilized to evaluate the detection performance of the waveform, which can be computed by

$$\text{PSL}(f_d) = 10\log_{10}\left(\frac{\max\limits_{k\neq 0} R_r^2(\boldsymbol{S}, k, f_d)}{R_r^2(\boldsymbol{S}, 0, f_d)}\right) \tag{14}$$

$$\text{ISL}(f_d) = 10\log_{10}\left(\frac{\sum\limits_{k=-L+1, k\neq 0}^{k=L-1} R_r^2(\boldsymbol{S}, k, f_d)}{R_r^2(\boldsymbol{S}, 0, f_d)}\right). \tag{15}$$

Obviously, the $\text{PSL}(f_d)$ and $\text{ISL}(f_d)$ are affected by the Doppler frequency f_d. In order to achieve a good detection ability of both stationary and moving targets, the $\text{PSL}(f_d)$ and $\text{ISL}(f_d)$ are expected to be low for $\forall f_d$.

D. The Correlation Property and Doppler Intolerance

When $f_d = 0$, it is found from (7) that the auto-ambiguity function of s_m becomes the autocorrelation function of s_m, and the cross-ambiguity function between s_m and s_n becomes the crosscorrelation function between s_m and s_n, given as

$$R_a(s_m) \triangleq \int_{-\infty}^{+\infty} s_m(t)s_m^*(t+\tau)dt = \chi_{s_m}(\tau, 0) \tag{16}$$

This article has been accepted for publication in a future issue of this journal, but has not been fully edited. Content may change prior to final publication. Citation information: DOI 10.1109/ACCESS.2018.2859404, IEEE Access

$$R_c(s_m, s_n) \triangleq \int_{-\infty}^{+\infty} s_n(t) s_m^*(t+\tau) dt = \chi_{s_m,s_n}(\tau, 0). \quad (17)$$

For the sampled signal $s_m(lT_s)$, by substituting $f_d = 0$ into (9) and (12), and ignoring the impact of the carrier frequency f_0, the $R_a(s_m, k)$ and $R_c(s_m, s_n, k)$ can be further written as

$$\begin{aligned} R_a(s_m, k) =& \chi_{s_m}(kT_s, 0) \\ =& R_{as}(\boldsymbol{a}_m, k) + R_{as}(\boldsymbol{b}_m, k) \\ \triangleq& R_{aa}(\boldsymbol{a}_m, \boldsymbol{b}_m, k) \end{aligned} \quad (18)$$

$$\begin{aligned} R_c(s_m, s_n, k) =& \chi_{s_m,s_n}(kT_s, 0) \\ =& R_{cs}(\boldsymbol{a}_m, \boldsymbol{a}_n, k) + R_{cs}(\boldsymbol{b}_m, \boldsymbol{b}_n, k) \\ \triangleq& R_{cc}(\boldsymbol{a}_m, \boldsymbol{a}_n, \boldsymbol{b}_m, \boldsymbol{b}_n, k) \end{aligned} \quad (19)$$

where the autocorrelation and crosscorrelation functions of the phase-coded sequences $\boldsymbol{a}_m, m = 1, 2, \cdots, M_t$ can be obtained by

$$\begin{aligned} &R_{as}(\boldsymbol{a}_m, k) = \chi_{a_m}(kT_s, 0) \\ &= \frac{1}{L} \sum_{l=0}^{L-|k|-1} \left[\exp\left(j a_m(l)\right) \exp\left(-j a_m(l+|k|)\right)\right] \end{aligned} \quad (20)$$

$$\begin{aligned} &R_{cs}(\boldsymbol{a}_m, \boldsymbol{a}_n, k) = \chi_{a_m,a_n}(kT_s, 0) \\ &= \frac{1}{L} \sum_{l=0}^{L-|k|-1} \left[\exp\left(j a_n(l)\right) \exp\left(-j a_m(l+|k|)\right)\right]. \end{aligned} \quad (21)$$

The $R_{as}(\boldsymbol{b}_m, k)$ and $R_{cs}(\boldsymbol{b}_m, \boldsymbol{b}_n, k)$ can be directly obtained by replacing the code sequence $\boldsymbol{a}_m$ and $\boldsymbol{a}_n$ in (20) and (21) by $\boldsymbol{b}_m$ and $\boldsymbol{b}_n$ respectively. By substituting (18) and (19) into (8), the synthetic output of the M_t matched filters for zero Doppler frequency can be written as

$$\begin{aligned} R_r(\boldsymbol{S}, 0) \triangleq& \sum_{m=1}^{M_t} |R_{rm}(s_m, \boldsymbol{S}, 0)| \\ =& \sum_{m=1}^{M_t} \left| R_a(s_m, k) + \sum_{n \neq m, n=1}^{M_t} R_c(s_m, s_n, k) \right|. \end{aligned} \quad (22)$$

The synthetic output $R_r(\boldsymbol{S}, 0)$ embodies the overall correlation properties (the autocorrelation and crosscorrelation properties) of the transmitted waveform set $\boldsymbol{S}$. The $R_a(s_m, k)$ is the main part of $R_r(\boldsymbol{S}, 0)$, and is expected to be a Dirac delta function. The $R_c(s_m, s_n, k)$ is usually viewed as the interference in $R_r(\boldsymbol{S}, 0)$, and is expected to be zero. Thus the $R_r(\boldsymbol{S}, 0)$ is desired to be a Dirac delta function with zero sidelobe level, i.e. PSL$(0) \approx 0$ and ISL$(0) \approx 0$.

To achieve the ideal synthetic output $R_r(\boldsymbol{S}, 0)$, it is found from the relations in (18) and (19) that the correlation properties of the phase-coded sequences $\{\boldsymbol{a}_m, \boldsymbol{b}_m, m = 1, 2, \cdots, M_t\}$ should be optimized. Specifically, the sidelobe level of $R_{aa}(\boldsymbol{a}_m, \boldsymbol{b}_m, k)$ should be suppressed, and the crosscorrelation level of $R_{cc}(\boldsymbol{a}_m, \boldsymbol{a}_n, \boldsymbol{b}_m, \boldsymbol{b}_n, k)$ should be reduced. Thus, we consider to design good phase-coded sequences at the transmitter to satisfy these requirements.

When $f_d \neq 0$, the good waveform performance can be broken by the nonzero Doppler frequency. This effect is called the Doppler intolerance of waveforms, which is a serious problem especially for phase-coded waveforms. By comparing (11) with (20) and comparing (13) with (21), a phase shift $\exp(j2\pi f_d l T_s)$ is induced by the nonzero f_d within a pulse. This intrapulse phase shift can break the autocorrelation and crosscorrelation properties of the phase-coded sequences in a single pulse. By comparing (9) with (18) and comparing (12) with (19), a phase shift $\exp(j2\pi f_d T_r)$ is induced by the nonzero f_d between different pulses. This interpulse phase shift can further break the sum properties of the autocorrelation and crosscorrelation functions of the phase-coded sequences in consecutive pulses.

These Doppler phase shifts raise the sidelobe level of the synthetic output, and reduce the detection ability for moving targets. When $|f_d|$ increases, the PSL(f_d) and ISL(f_d) become much higher than the PSL(0) and ISL(0). In general, the PSL(f_d) and ISL(f_d) are utilized as the measurable indicator for the Doppler intolerance. If the PSL(f_d) and ISL(f_d) remain almost unchanged or increase slowly with the increased $|f_d|$, we regard that the good Doppler tolerance of the waveforms is gained. The good Doppler tolerance can be indicated by

$$\text{PSL}(f_d) \approx \text{PSL}(0), \forall f_d \neq 0 \quad (23)$$

$$\text{ISL}(f_d) \approx \text{ISL}(0), \forall f_d \neq 0. \quad (24)$$

Since the optimization of a set of waveforms with good Doppler tolerance at the transmitter is computationally complex, we consider to compensate the Doppler phase shift by signal processing techniques at the receiver for obtaining a good Doppler tolerance.

III. Waveform Optimization

A. Suppressing the Autocorrelation Sidelobes by Optimizing the Complementary Chaotic Phase-Coded Waveforms

An effective method to suppress the autocorrelation sidelobes of phase-coded waveforms is to utilize the complementary sequences. A pair or set of sequences is identified as complementary sequences (CSs) if and only if the sum of the aperiodic autocorrelation functions of the sequences is an ideal Dirac delta function [45]. The CSs are usually modulated on consecutive pulses in a coherent pulse train, which overcomes the difficulty of realizing the ideal autocorrelation function in only one pulse. However, the number, code length, and phase number of the existing complementary sequences are fixed, e.g., the Golay [24] and Frank [46] sequences. To break this limitation and flexibly choose the parameters of the complementary sequences, we consider to optimize the complementary architecture based on chaotic phase-coded sequences. By utilizing appropriate optimization algorithms, the approximate complementary chaotic phase-coded sequences are obtained. Thus the autocorrelation sidelobes can be greatly suppressed, and many side benefits are gained from the chaotic properties.

Firstly, the optimization problem is formulated. Ideally, for strictly complementary codes, when the Doppler frequency is

This article has been accepted for publication in a future issue of this journal, but has not been fully edited. Content may change prior to final publication. Citation information: DOI 10.1109/ACCESS.2018.2859404, IEEE Access

zero, the $\boldsymbol{a}_m$ and $\boldsymbol{b}_m$ satisfy the following equation

$$\begin{aligned} R_{aa}\left(\boldsymbol{a}_m, \boldsymbol{b}_m, k\right) =& R_{as}\left(\boldsymbol{a}_m, k\right) + R_{as}\left(\boldsymbol{b}_m, k\right) \\ =& \begin{cases} 2, & k = 0 \\ 0, & k = \pm 1, \pm 2, \cdots, \pm\left(L-1\right) \end{cases} \end{aligned} \tag{25}$$

where k is the delay point of the autocorrelation function.

Actually, sequence pairs that strictly satisfy the equation of (25) mathematically are limited. All those pairs previously found are exhaustively searched by computers. For long and complex complementary sequences, an intolerable amount of computation is required. Thus we relax the restriction of (25), and build an approximate model to approach it. Specifically, the sum of the autocorrelation functions of $\boldsymbol{a}_m$ and $\boldsymbol{b}_m$ is firstly calculated, which is $R_{aa}(\boldsymbol{a}_m, \boldsymbol{b}_m, k)$. Then, the peak sidelobe level (PSL) and the integrated sidelobe level (ISL) of $R_{aa}(\boldsymbol{a}_m, \boldsymbol{b}_m, k)$ are computed as

$$\mathrm{PSL}_{R_{aam}} = 10\log_{10}\left(\frac{\max\limits_{k\neq 0} R_{aa}^2(\boldsymbol{a}_m, \boldsymbol{b}_m, k)}{R_{aa}^2(\boldsymbol{a}_m, \boldsymbol{b}_m, 0)}\right) \tag{26}$$

$$\mathrm{ISL}_{R_{aam}} = 10\log_{10}\left(\frac{\sum\limits_{k=-L+1, k\neq 0}^{k=L-1} R_{aa}^2(\boldsymbol{a}_m, \boldsymbol{b}_m, k)}{R_{aa}^2(\boldsymbol{a}_m, \boldsymbol{b}_m, 0)}\right). \tag{27}$$

The PSL and ISL should be minimized (ideally to zero) to approach the equation of (25). To further simplify the computation, the first sequence of $\boldsymbol{a}_m$ is pre-given, and the corresponding sequence of $\boldsymbol{b}_m$ is searched. Then, the cost function is constructed as

$$E_{um}(\boldsymbol{b}_m) = \mathrm{ISL}_{R_{aam}} + \mu \mathrm{PSL}_{R_{aam}} \tag{28}$$

where μ is the weight coefficient balancing the PSL and the ISL. The problem for finding the optimal complementary sequence $\boldsymbol{b}_m$ corresponding to $\boldsymbol{a}_m$ is formulated as

$$\begin{aligned} &\min_{\boldsymbol{b}_m} E_{um}(\boldsymbol{b}_m), m = 1, 2, \cdots, M_t \\ &s.t. \quad b_m(l) \in \left\{0, \frac{2\pi}{M_c}, 2\frac{2\pi}{M_c}, \cdots, (M_c-1)\frac{2\pi}{M_c}\right\}. \end{aligned} \tag{29}$$

By solving this optimization problem, the sequence pair of $\boldsymbol{a}_m$ and $\boldsymbol{b}_m$ approximately satisfying (25) can be found.

The above non-linear optimization problem is a NP-complete problem. The traditional greedy algorithms are often easy to get trapped in a local optimum because they search along the directions to reduce the cost function. The greedy algorithms are very limited for solving this kind of problems. In contrast, the statistical optimization algorithms [47] provide effective solving method. The searching for complementary sequences is very similar with the immune process. Thus, in this paper, the adaptive clonal selection (ACS) algorithm is utilized. Moveover, the algorithm's advantages in the fast convergence speed and efficient global optimization ability for solving the NP problem are obtained.

The adaptive clonal selection algorithm is inspired by the biology immune system. By simulating the mechanisms of self-adjusting, learning and adapting in the natural immune system, the algorithm realizes the global optimal solution. The antigen corresponds to the cost function under different constraints of the optimization problem, and the antibody corresponds to the optimal solution of the optimization problem. The affinity function of the antigen and antibody corresponds to the matching degree between the solution of the optimization problem and the cost function. In the algorithm, the clonal scale of the antibody population, the mutation probability of the antibody, and the selection probability of the mutation are adaptively adjusted to enhance the diversity of the population, increase convergence speed, and avoid the premature convergence.

Assuming that $\boldsymbol{a}_m$ is pre-given, and the sequence $\boldsymbol{b}_m$ having the maximum affinity value is searched. There are mainly seven steps in the algorithm, which are described specifically as follows.

1) **Population initialization**
A chaotic map is chosen, and a chaotic phase-coded sequence ${\boldsymbol{a}_m}^T$ with size of $1 \times L$ is generated by using the method described in Sec.II.B. Then the initial values of this chosen chaotic map are changed, and the generation operations are repeated by N_p times to get a set of chaotic phase-coded sequences $\boldsymbol{b}_m(i) = [b_{m1}(i), b_{m2}(i), \cdots, b_{ml}(i), \cdots, b_{mL}(i)]^T$, where $i = 1, 2, \cdots, N_p$. An antibody is defined as $\boldsymbol{\beta}_i = \boldsymbol{b}_m(i)$, then the initial population is

$$\begin{aligned} \boldsymbol{\Theta}(n\,|n=0\,) =& \{\boldsymbol{\beta}_1(n=0), \boldsymbol{\beta}_2(n=0), \\ & \cdots, \boldsymbol{\beta}_{N_p}(n=0)\} \\ \triangleq& \{\boldsymbol{\beta}_i(n=0)\}_{i=1,2,\cdots,N_p}. \end{aligned} \tag{30}$$

2) **Affinities calculation and ordering**
An affinity function is defined by $H(\boldsymbol{\beta}_i) = 1/E_{um}(\boldsymbol{b}_m(i))$. For each antibody $\boldsymbol{\beta}_i$, their affinity functions are calculated, then their values are ranked in a descending order, given as

$$\begin{aligned} &\{\boldsymbol{\beta}_1^{\circ}(n), \boldsymbol{\beta}_2^{\circ}(n), \cdots, \boldsymbol{\beta}_{N_p}^{\circ}(n)| \\ &H(\boldsymbol{\beta}_1^{\circ}(n)) \geq H(\boldsymbol{\beta}_2^{\circ}(n)) \geq \cdots \geq H(\boldsymbol{\beta}_{N_p}^{\circ}(n))\}. \end{aligned} \tag{31}$$

3) **Clonal operation**
According to the affinity value of each antibody, the clone scale of the ith antibody is decided by

$$q_i(n) = \mathrm{ceil}(n_c H(\boldsymbol{\beta}_i(n)) / \sum_{i=1}^{N_p} H(\boldsymbol{\beta}_i(n))) \tag{32}$$

where n_c is the parameter on determining the clonal size. After the clonal operation, the new population becomes

$$\boldsymbol{\Theta}^{'}(n\,|n=0\,) = \{{\boldsymbol{\beta}^{'}}_{iq}(n)\}_{\substack{i=1,2,\cdots,N_p \\ q=1,2,\cdots q_i(n)}}. \tag{33}$$

4) **Mutation operation**
The mutation probability p_{iq} of the cloned antibody ${\boldsymbol{\beta}^{'}}_{iq}(n)$ is adjusted according to its affinity value and the evolutionary generation n. The adaptive mutation probability is chosen as

$$p_{iq} = \begin{cases} p_{\max} - \left(\frac{p_{\max}-p_{\min}}{N}\right) n, & H({\boldsymbol{\beta}^{'}}_{iq}(n)) > H_{avg} \\ p_{\max}, & H({\boldsymbol{\beta}^{'}}_{iq}(n)) \leq H_{avg} \end{cases} \tag{34}$$

This article has been accepted for publication in a future issue of this journal, but has not been fully edited. Content may change prior to final publication. Citation information: DOI 10.1109/ACCESS.2018.2859404, IEEE Access

where $p_{\max}$ is the maximum mutation probability, and $p_{\min}$ is the minimum mutation probability. N is the total number of generations, and n presents the current generation. $H(\boldsymbol{\beta}^{'}_{iq}(n))$ is the affinity value of the evolving antibody $\boldsymbol{\beta}^{'}_{iq}(n)$, and H_{avg} is the average affinity value of the population.

5) **Clone selection operation**
An optimal antibody is selected from the mutated antibodies according to the affinity values, given as

$$\begin{aligned}\boldsymbol{\kappa}_i(n) &= \boldsymbol{\beta}^{'}_{iq}(n) \left| \max H(\boldsymbol{\beta}^{'}_{iq}(n)) \right. \\ q &= 1, 2, \cdots, q_i, i = 1, 2, \cdots, N_p. \end{aligned} \tag{35}$$

The new antibody replaces the original antibody with a probability of

$$\begin{aligned} & p_s^n(\boldsymbol{\beta}_i(n) \to \boldsymbol{\kappa}_i(n)) \\ =& \begin{cases} 0, & H(\boldsymbol{\kappa}_i(n)) < H(\boldsymbol{\beta}_i(n)) \\ \exp\left(\frac{H(\boldsymbol{\kappa}_i(n)) - H(\boldsymbol{\beta}_i(n))}{\zeta}\right) & H(\boldsymbol{\kappa}_i(n)) \geq H(\boldsymbol{\beta}_i(n)), \\ & \boldsymbol{\beta}_i(n) \text{ is not optimal} \\ 1, & H(\boldsymbol{\kappa}_i(n)) \geq H(\boldsymbol{\beta}_i(n)), \\ & \boldsymbol{\beta}_i(n) \text{ is optimal} \end{cases} \end{aligned} \tag{36}$$

where ζ is a parameter related to the population diversity. A large ζ implies a more diverse population.

6) **Population regeneration**
The generation of the evolution becomes $n = n+1$, and the population regenerates into

$$\begin{aligned} \boldsymbol{\Theta}(n+1) =& \{\boldsymbol{\beta}_1(n+1), \boldsymbol{\beta}_2(n+1), \\ & \cdots, \boldsymbol{\beta}_{N_p}(n+1)\} \\ \triangleq& \{\boldsymbol{\beta}_i(n+1)\}_{i=1,2,\cdots,N_p}. \end{aligned} \tag{37}$$

7) **The termination condition**
If the generation number reaches N, the iteration is terminated. The antibody of the current population having the largest affinity value is retained. Then the optimal complementary chaotic phase coded sequence $\boldsymbol{b}_m$ corresponding with $\boldsymbol{a}_m$ is obtained. Otherwise, it turns to step (2).

If the above operations are repeated with different initial values by M_t times, M_t chaotic phase-coded complementary pairs $\{\boldsymbol{a}_m, \boldsymbol{b}_m\}_{m=1,2,\cdots,M_t}$ are randomly and independently obtained. The crosscorrelation between different pairs is small, and the M_t complementary pairs are quasi-orthogonal.

The above optimization strategy can significantly reduce the computational load, and can ensure the superior waveform performance with good autocorrelation and crosscorrelation properties. If the autocorrelation and crosscorrelation properties are jointly optimized, the computation cost for exhaustively searching the orthogonal set of phase-coded waveforms is on the order of $M_c^{M_t L}$. For the optimization strategy proposed in this paper, the computation cost of exhaustively searching is on the order of $M_t M_c^L$. It is seen that the computation cost of our method is lower than that of the existing methods.

B. Eliminating the Waveform Crosscorrelation by the Space-Time Coding

To further eliminate the crosscorrelation between different transmitted waveforms, the space-time coding is implemented on the pulse trains of complementary chaotic sequences for obtaining the multidimensional waveforms for MIMO radar applications.

The space-time coding was first applied in wireless communication systems to significantly improve the reliability of communications by transmitting signals from different antennas in fading channels [48]. In a wireless communication system with two transmitters and two receivers, the signals transmitted in the first time periods of antenna 1 and antenna 2 are $\boldsymbol{s}_1$ and $\boldsymbol{s}_2$, then the space-time coding rules [49] are

$$(\boldsymbol{s}_1, \boldsymbol{s}_2) \to \boldsymbol{S} = \begin{pmatrix} \boldsymbol{s}_1 & -\boldsymbol{s}_2^* \\ \boldsymbol{s}_2 & \boldsymbol{s}_1^* \end{pmatrix} \begin{matrix} \to \text{Time dimension} \\ \downarrow \text{Space dimension} \end{matrix} \tag{38}$$

where the superscript $*$ denotes the complex conjugate. Different rows of (38) represent the waveforms transmitted from different antennas, and different columns represent the waveforms transmitted in different PRIs. At the receiver, $\boldsymbol{S}^H$ is used to decode the signal, and the superscript H denotes the complex conjugate transposition.

The complementary chaotic phase-coded sequences of $\boldsymbol{a}_m$ and $\boldsymbol{b}_m$ are assumed to constitute the basic transmitted waveforms. Then the complementary space-time coding is implemented on the basic transmitted waveforms as

$$\boldsymbol{S}_{2\times 2} = \begin{pmatrix} \boldsymbol{a}_m{}^T & \boldsymbol{b}_m{}^H \boldsymbol{J}_L \\ \boldsymbol{b}_m{}^T & -\boldsymbol{a}_m{}^H \boldsymbol{J}_L \end{pmatrix} \begin{matrix} \to \text{Time dimension} \\ \downarrow \text{Space dimension} \end{matrix} \tag{39}$$

where $\boldsymbol{J}_L$ represents a $L \times L$ exchanging matrix with ones on its antidiagonal and zeros elsewhere. This space-time coding matrix can be expanded into the 4×4 dimension as in (40), where $[\cdot]_{2\times 2}^H$ represents the block Hermitian transposition for a 2×2 block matrix. $\boldsymbol{S}_{4\times 4}$ contains the chaotic phase-coded sequences with STCC transmitted from four antennas. Obviously, any $2^p \times 2^p$ ($p \geq 2$, and p is an integer) matrix based on the chaotic phase-coded sequences with STCC can be constructed from the $2^{p-1} \times 2^{p-1}$ matrix recursively as

$$\boldsymbol{S}_{2^p\times 2^p} = \begin{pmatrix} \boldsymbol{S}_{2^{p-1}\times 2^{p-1}} & [\boldsymbol{S}_{2^{p-1}\times 2^{p-1}} \boldsymbol{J}_{2^{p-1}L}]_{2^{p-1}\times 2^{p-1}}^H \\ \boldsymbol{S}_{2^{p-1}\times 2^{p-1}} & -[\boldsymbol{S}_{2^{p-1}\times 2^{p-1}} \boldsymbol{J}_{2^{p-1}L}]_{2^{p-1}\times 2^{p-1}}^H \end{pmatrix}. \tag{41}$$

$$\boldsymbol{S}_{4\times 4} = \begin{pmatrix} \boldsymbol{S}_{2\times 2} & [\boldsymbol{S}_{2\times 2} \boldsymbol{J}_{2L}]_{2\times 2}^H \\ \boldsymbol{S}_{2\times 2} & -[\boldsymbol{S}_{2\times 2} \boldsymbol{J}_{2L}]_{2\times 2}^H \end{pmatrix} = \begin{pmatrix} \boldsymbol{a}_m{}^T & \boldsymbol{b}_m{}^H \boldsymbol{J}_L & \boldsymbol{a}_m{}^H \boldsymbol{J}_L & \boldsymbol{b}_m{}^H \boldsymbol{J}_L \\ \boldsymbol{b}_m{}^T & -\boldsymbol{a}_m{}^H \boldsymbol{J}_L & \boldsymbol{b}_m{}^T & -\boldsymbol{a}_m{}^T \\ \boldsymbol{a}_m{}^T & \boldsymbol{b}_m{}^H \boldsymbol{J}_L & -\boldsymbol{a}_m{}^H \boldsymbol{J}_L & -\boldsymbol{b}_m{}^H \boldsymbol{J}_L \\ \boldsymbol{b}_m{}^T & -\boldsymbol{a}_m{}^H \boldsymbol{J}_L & -\boldsymbol{b}_m{}^T & \boldsymbol{a}_m{}^T \end{pmatrix} \begin{matrix} \to \text{Time dimension} \\ \downarrow \text{Space dimension} \end{matrix} \tag{40}$$

This article has been accepted for publication in a future issue of this journal, but has not been fully edited. Content may change prior to final publication. Citation information: DOI 10.1109/ACCESS.2018.2859404, IEEE Access

Hereinafter, we assume that the transmitted sequence set is $\boldsymbol{S}_{4\times4}$, which means that the number of transmitted waveforms is $M_t = 4$, and that the number of transmitted pulses in a coherent train is $N = 4$. Then the sampled transmitted waveform matrix can be presented as

$$\boldsymbol{S}(l) = \begin{pmatrix} \boldsymbol{a}_m(l) & \boldsymbol{b}_m{}^*(-l) & \boldsymbol{a}_m{}^*(-l) & \boldsymbol{b}_m{}^*(-l) \\ \boldsymbol{b}_m(l) & -\boldsymbol{a}_m{}^*(-l) & \boldsymbol{b}_m(l) & -\boldsymbol{a}_m(l) \\ \boldsymbol{a}_m(l) & \boldsymbol{b}_m{}^*(-l) & -\boldsymbol{a}_m{}^*(-l) & -\boldsymbol{b}_m{}^*(-l) \\ \boldsymbol{b}_m(l) & -\boldsymbol{a}_m{}^*(-l) & -\boldsymbol{b}_m(l) & \boldsymbol{a}_m(l) \end{pmatrix} \tag{42}$$

where different rows represent waveform samples transmitted from different antennas, and different columns represent waveform samples in different PRIs. If the target delay is at the k_tth sample, then the received signal $\boldsymbol{x}^T(l)$ in four PRIs at a certain receiving antenna is

$$\boldsymbol{x}^T(l) = \boldsymbol{h}^T\boldsymbol{S}(l-k_t)\boldsymbol{D} + \boldsymbol{n}^T(l) \tag{43}$$

where $\boldsymbol{x}^T(l) = [x_1(l), x_2(l), x_3(l), x_4(l)]$ is a 1×4 row vector, and $x_i(l)$ is the sampled signal received in the ith PRI. $\boldsymbol{h}^T = [h_1, h_2, h_3, h_4]$ contains the coefficients of the propagation channels corresponding to those four transmitted waveforms. $\boldsymbol{n}^T(l) = [n_1(l), n_2(l), n_3(l), n_4(l)]$ is the received noise in four PRIs. $\boldsymbol{D} = diag\{1, e^{j\theta}, e^{j2\theta}, e^{j3\theta}\}$ is the Doppler phase shift matrix, where $\theta = 2\pi f_d T_r$ is the interpulse phase shift induced by the Doppler frequency f_d. As in most cases, the intrapulse Doppler phase shift is ignored here. For the waveforms transmitted in a pulse train, the received signal in each PRI is matched filtering first, then the matched filtering results of the successive PRIs are coherently accumulated. This process can be expressed by the following equation

$$\begin{aligned}\boldsymbol{r}^T(k) =& \sum_{i=1}^{4} x_i(l) \otimes \boldsymbol{s}_i{}^H(-l) = \sum_{i=1}^{4}[\sum_{l=-\infty}^{+\infty} x_i(l)\boldsymbol{s}_i^H(k+l)] \\ =& \boldsymbol{x}^T(l) \otimes \boldsymbol{S}^H(-l)\end{aligned} \tag{44}$$

where $k = -(L-1), \cdots, (L-1)$. $\boldsymbol{s}_i(l)$ is a column vector representing the M_t waveforms transmitted in the ith PRI, and $\boldsymbol{S}(l) = [\boldsymbol{s}_1(l), \boldsymbol{s}_2(l), \boldsymbol{s}_3(l), \boldsymbol{s}_4(l)]$. The subscript i represents the ith PRI. $\boldsymbol{r}^T(k) = [r_1(k), r_2(k), r_3(k), r_4(k)]$ is a 1×4 row vector, and $r_j(k)$ is the matched filtering result corresponding to the jth transmitted waveform. The $\otimes$ represents the convolution. By substituting (43) into (44), we have

$$\boldsymbol{r}^T(k) = \boldsymbol{h}^T\boldsymbol{S}(l-k_t)\boldsymbol{D} \otimes \boldsymbol{S}^H(-l) + \boldsymbol{n}^T(l) \otimes \boldsymbol{S}^H(-l). \tag{45}$$

If $f_d = 0$, we have $\boldsymbol{D} = \boldsymbol{I}$, then (45) becomes

$$\boldsymbol{r}^T(k) = \boldsymbol{h}^T\boldsymbol{S}(l-k_t) \otimes \boldsymbol{S}^H(-l) + \boldsymbol{n}^T(l) \otimes \boldsymbol{S}^H(-l). \tag{46}$$

Benefiting from the STCC, we have

$$\boldsymbol{S}(l-k_t) \otimes \boldsymbol{S}^H(-l) = 4L\boldsymbol{I}_4\delta(k-k_t) \tag{47}$$

where $\boldsymbol{I}_4$ is a 4×4 identity matrix. By substituting (47) into (46), the matched filtering results become

$$\boldsymbol{r}^T(k) = 4L\boldsymbol{h}^T\delta(k-k_t) + \boldsymbol{n}^T(l) \otimes \boldsymbol{S}^H(-l). \tag{48}$$

From (48), it is found that after the matched filtering and coherent accumulation on the received signal, the crosscorrelation between different waveforms is eliminated, and the sidelobes of the autocorrelation are also reduced due to the STCC property. $\boldsymbol{r}^T(k)$ is a vector containing the matched filtering results corresponding to $M_t = 4$ waveforms. We combine the results of the $M_t = 4$ matched filters, and obtain the synthetic output, given as

$$R_r(\boldsymbol{S}, k) = \left\|\boldsymbol{r}^T(k)\right\|_1, k = -(L-1), \cdots, (L-1) \tag{49}$$

where $\|\cdot\|_1$ is the ℓ_1 norm. We utilize the synthetic output as the detection function to detect targets. Obviously, $R_r(\boldsymbol{S}, k)$ in (49) is an approximate Dirac delta function with a maximum value at the target delay k_t. According to (14) and (15), we have PSL$(0) \approx 0$ and ISL$(0) \approx 0$. The sidelobe level of the synthetic output is very low, which is propitious to detect targets.

C. The Weighting Method for Doppler Intolerance Mitigation

When the target is moving, we have $f_d \neq 0$ and $\boldsymbol{D} \neq \boldsymbol{I}$. Then the STCC property is broken by the nonzero Doppler frequency f_d, given as

$$\boldsymbol{S}(l-k_t)\boldsymbol{D} \otimes \boldsymbol{S}^H(-l) \neq 4L\boldsymbol{I}_4\delta(k-k_t). \tag{50}$$

In this case, the crosscorrelation in $\boldsymbol{S}$ cannot be eliminated, and the sidelobes of the autocorrelation functions also rise. If the traditional accumulation method described in (49) is utilized to detect targets, the high range sidelobes caused by the imperfect crosscorrelation and imperfect autocorrelation properties deteriorate the target detection performance and result in a high false probability. In order to depress the affect of the Doppler frequency and mitigate the Doppler intolerance of the waveforms, a weighting method by using an estimated null space vector in [50] is introduced to compensate the interpulse Doppler phase shift.

When $f_d = 0$ and the noise is ignored for convenience, we denote the received signal in different PRIs as $\boldsymbol{x}^{\circ T}(l) = [x_1^\circ(l), x_2^\circ(l), x_3^\circ(l), x_4^\circ(l)] = \boldsymbol{h}^T\boldsymbol{S}(l-k_t)$. When $f_d \neq 0$ and the noise is ignored for convenience, the received signal in different PRIs can be written as

$$\begin{aligned}\boldsymbol{x}^T(l) &= \boldsymbol{x}^{\circ T}(l)\boldsymbol{D} \\ &= [x_1^\circ(l), x_2^\circ(l)e^{j\theta}, x_3^\circ(l)e^{j2\theta}, x_4^\circ(l)e^{j3\theta}].\end{aligned} \tag{51}$$

If the interpulse Doppler phase shift of the received signal in (51) is compensated by a weighting vector $\boldsymbol{w}_d = [1, e^{j\theta}, e^{j2\theta}, e^{j3\theta}]^T$, the Doppler affect on the STCC can be eliminated. The compensated received signal can be written as $\boldsymbol{x}_c^T(l) = \boldsymbol{w}_d^H \odot \boldsymbol{x}^T(l)$, where the $\odot$ is the Hadamard product. If the weighting vector $\boldsymbol{w}_d$ is accurate, the compensated received signal is equal to the received signal without Doppler modulation as $\boldsymbol{x}_c^T(l) = \boldsymbol{x}^{\circ T}(l)$. However, for an unknown target, f_d is unknown. Thus, the weighting vector $\boldsymbol{w}_d$ or the Doppler phase shift $\theta = 2\pi f_d T_r$ should be estimated first.

This article has been accepted for publication in a future issue of this journal, but has not been fully edited. Content may change prior to final publication. Citation information: DOI 10.1109/ACCESS.2018.2859404, IEEE Access

If the matched filtering results of those four pulses in (44) are arranged in a column, a compressed data matrix can be written as

$$\boldsymbol{E}(k)=\begin{bmatrix} x_1(l)\otimes \boldsymbol{s}_1{}^H(-l) \\ x_2(l)\otimes \boldsymbol{s}_2{}^H(-l) \\ x_3(l)\otimes \boldsymbol{s}_3{}^H(-l) \\ x_4(l)\otimes \boldsymbol{s}_4{}^H(-l) \end{bmatrix}. \tag{52}$$

Then (44) is equivalent to

$$\boldsymbol{r}^T(k)=\boldsymbol{w}^H\boldsymbol{E}(k) \tag{53}$$

where $\boldsymbol{w}=[1,1,1,1]^T$. When $f_d=0$, we can obtain the following equation from (48) as

$$\boldsymbol{w}^H\boldsymbol{E}(k)=4L\boldsymbol{h}^T\delta(k-k_t) \tag{54}$$

where noise is ignored for convenience. When $f_d\neq 0$, (54) cannot be hold. If we weight the received signals in different PRIs as $\boldsymbol{w}_d^H\odot\boldsymbol{x}^T(l)$ and substitute them into the matched filters in (52), a new equation can be obtained as

$$\boldsymbol{w}_d{}^H\boldsymbol{E}(k)=4L\boldsymbol{h}^T\delta(k-k_t). \tag{55}$$

(55) can be regarded as weighting the matched filtering results in different PRIs, and the equation ensures the effectiveness of the STCC in our designed waveforms. It is found from (55) that if $k\neq k_t$, $\boldsymbol{w}_d$ lies in the null space of $\boldsymbol{E}(k)$. By the subspace decomposition, the null space vector $\hat{\boldsymbol{w}}_d$ can be estimated from $\boldsymbol{E}(k)$. However, if $k=k_t$, $\hat{\boldsymbol{w}}_d$ doesn't lie in the null space of $\boldsymbol{E}(k)$, and cannot be estimated from $\boldsymbol{E}(k)$. The target delay k_t is unknown, thus all the possible target delays should be considered to estimate the vector $\hat{\boldsymbol{w}}_d$.

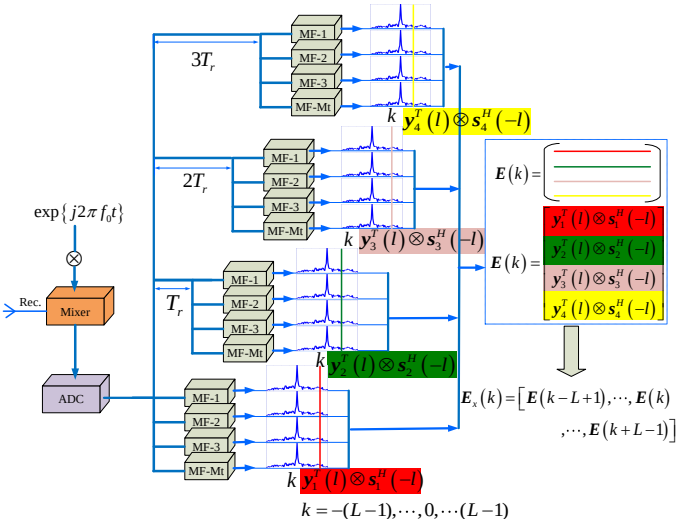

Fig. 1: The data arrangement process to obtain $\boldsymbol{E}_x(k)$

By referring to [50], the estimation procedures for $\hat{\boldsymbol{w}}_d$ are summarized as follows.

1) Construct an extended matrix $\boldsymbol{E}_x(k)$ from $\boldsymbol{E}(k)$ as

$$\boldsymbol{E}_x(k)=[\boldsymbol{E}(k-L+1),\cdots,\boldsymbol{E}(k),\cdots,\boldsymbol{E}(k+L-1)] \tag{56}$$

where $\boldsymbol{E}_x(k)$ is a $1\times(2L-1)$ block matrix. The data arrangement process for obtaining $\boldsymbol{E}_x(k)$ is shown in Fig. 1. Since the target delay k_t is unknown, $\boldsymbol{E}(k)$ at all possible delays are considered in $\boldsymbol{E}_x(k)$. The correlation matrix of $\boldsymbol{E}_x(k)$ is calculated by

$$\boldsymbol{R}_E(k)=\boldsymbol{E}_x(k)\boldsymbol{E}_x{}^H(k). \tag{57}$$

2) A trial-and-error method is utilized to eliminate the impact of $\boldsymbol{E}(k=k_t)$ for an unknown k_t. By subtracting the correlation matrix of $\boldsymbol{E}(h)$ from $\boldsymbol{R}_E(k)$, a new matrix is obtained as

$$\boldsymbol{R}_E{}'(h)=\boldsymbol{R}_E(k)-\boldsymbol{E}(h)\boldsymbol{E}^H(h) \tag{58}$$

where $h=(k-L+1),\cdots,k,\cdots,(k+L-1)$. The number of $\boldsymbol{R}_E{}'(h)$ is $2L-1$. The eigenvalue decomposition is performed on $\boldsymbol{R}_E{}'(h)$, and the eigenvectors corresponding to the minimum eigenvalue of each $\boldsymbol{R}_E{}'(h)$ are stored as $\boldsymbol{f}_1(k)$,$\boldsymbol{f}_2(k)$,...,$\boldsymbol{f}_{2L-1}(k)$.

3) By arranging these eigenvectors in a row, a new matrix $\boldsymbol{F}(k)=[\boldsymbol{f}_1(k),\boldsymbol{f}_2(k),\cdots,\boldsymbol{f}_{2L-1}(k)]$ is constructed. The optimal weighting vector for Doppler compensation is one of the column vectors in $\boldsymbol{F}(k)$. The inner product matrix of $\boldsymbol{F}(k)$ is computed by

$$\boldsymbol{G}(k)=\boldsymbol{F}^H(k)\boldsymbol{F}(k)=[\boldsymbol{g}_1,\boldsymbol{g}_2,\cdots,\boldsymbol{g}_{2L-1}]^T. \tag{59}$$

4) From $\boldsymbol{G}(k)$, the eigenvector in $\boldsymbol{F}(k)$ which has the minimum inner product with other eigenvectors can be indexed by

$$j=\arg\min_{j=1,2,\cdots,2L-1}\|\boldsymbol{g}_j\|_2 \tag{60}$$

where $\|\cdot\|_2$ is the ℓ_2 norm. Thus $\boldsymbol{f}_j(k)$ is the estimated weighting vector for Doppler compensation, i.e., $\hat{\boldsymbol{w}}_d=\boldsymbol{f}_j(k)$.

When the weighting vector $\hat{\boldsymbol{w}}_d$ is obtained, the matched filtering results in different PRIs are weighted as

$$\boldsymbol{r}_c^T(k)=\hat{\boldsymbol{w}}_d^H\boldsymbol{E}(k). \tag{61}$$

Similar to (49), the compensated synthetic output becomes

$$R_{rc}(\boldsymbol{S},k,f_d)=\|\boldsymbol{r}_c^T(k)\|_1=\left\|\hat{\boldsymbol{w}}_d^H\boldsymbol{E}(k)\right\|_1=\left\|\boldsymbol{f}_j{}^H(k)\boldsymbol{E}(k)\right\|_1 \tag{62}$$

where $k=-(L-1),\cdots,(L-1)$. According to (55), we have $\hat{\boldsymbol{w}}_d^H\boldsymbol{E}(k)\approx 4L\boldsymbol{h}^T\delta(k-k_t)$. Then, $R_{rc}(\boldsymbol{S},k,f_d)$ is approximate to be a Dirac delta function with a maximum value at the target delay k_t. By substituting $R_{rc}(\boldsymbol{S},k,f_d)$ into (14) and (15), we have $\mathrm{PSL}(f_d)\approx\mathrm{PSL}(0)\approx 0$ and $\mathrm{ISL}(f_d)\approx\mathrm{ISL}(0)\approx 0$, which indicates that the Doppler tolerance of the chaotic phase-coded waveforms with STCC is regained.

By optimizing at the transmitter and using the compensation manipulation at the receiver, the target can be detected with a small false alarm probability. The flowchart of the transmitted waveform design and received signal processing is shown in Fig. 2.

IV. Simulation and Analysis

To verify the effectiveness of our proposed waveform designing methodology, simulation results are presented in this section. Note that an arbitrary number of chaotic sequences with an arbitrary length and an arbitrary phase number can

This article has been accepted for publication in a future issue of this journal, but has not been fully edited. Content may change prior to final publication. Citation information: DOI 10.1109/ACCESS.2018.2859404, IEEE Access

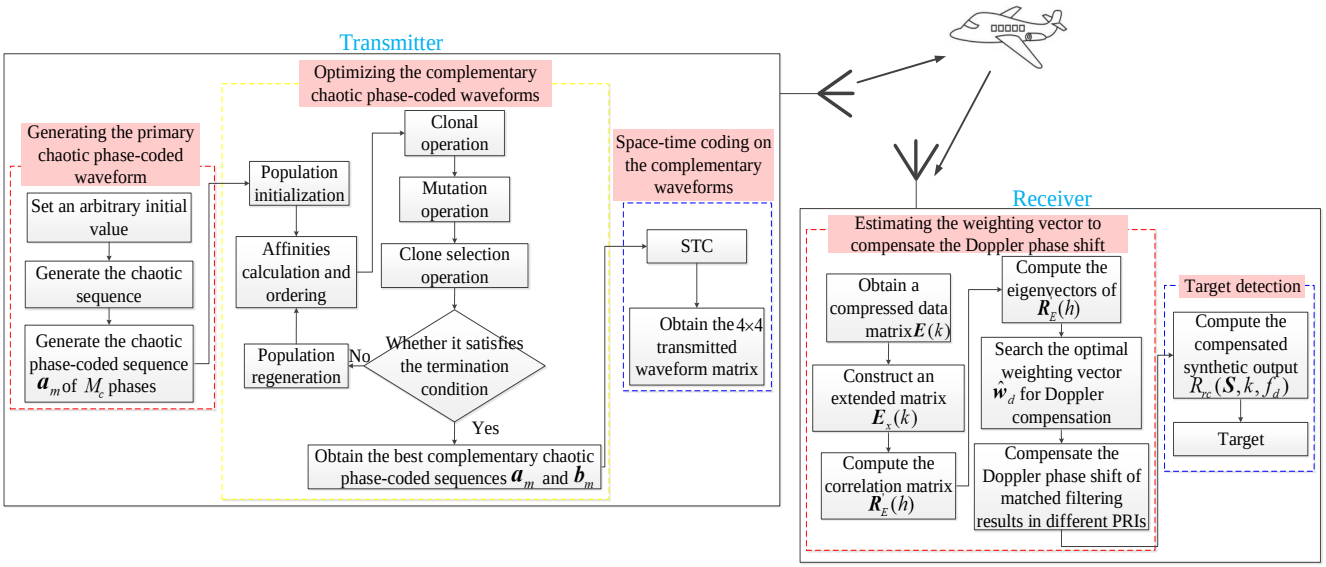

Fig. 2: The flowchart of the transmitted waveform design and received signal processing

be easily generated. The number of the transmitting antennas $M_t = 4$ and the sequence length $L = 40$ are used to illustrate our waveform design method. Four above-mentioned typical chaotic maps of logistic, Tent, hybrid logistic-tent, and hyper logistic are used to generate the basic chaotic sequences. These sequences are mapped into 4-ary phase-coded $\{0, \pi, \pi/2, 3\pi/2\}$ sequences, i.e., the phase number is $M_c = 4$. The Deng's codes proposed in [30] are used for comparison.

A. Primary Chaotic Phase-Coded Waveforms Generated by Four Typical Chaotic Maps

Four kinds of primary chaotic phase-coded waveforms are generated from chaotic maps of logistic, tent, hybrid logistic-tent, and hyper logistic with random initial values. Here, four kinds of primary chaotic waveform sets composed of $M_t = 4$ phase-coded sequences are transmitted directly. The synthetic outputs $R_r(\boldsymbol{S}) = R_r(\boldsymbol{S}, 0)$ of them are computed according to (22), and a random trial of those four synthetic outputs is demonstrated in Fig. 3.

The synthetic outputs represent the pulse compression results for MIMO radars, which indicate the correlation properties of the chaotic phase-coded waveforms. It is found from Fig. 3 that: (1) The sidelobe levels of the synthetic outputs for those four kinds of primary chaotic phase-coded waveforms are relatively high, thus they cannot be directly applied as detection waveforms for MIMO radars. (2) Different kinds of chaotic phase-coded waveforms have different correlation properties. For instance, the hyper logistic and tent phase-coded waveforms have relatively the best synthetic outputs, and the logistic phase-coded waveforms have almost the worst synthetic outputs. (3) The correlation properties of the primary chaotic phase-coded waveforms should be further optimized. The primary chaotic sequences with better initial correlation properties (or better synthetic outputs) can obtain better optimization results.

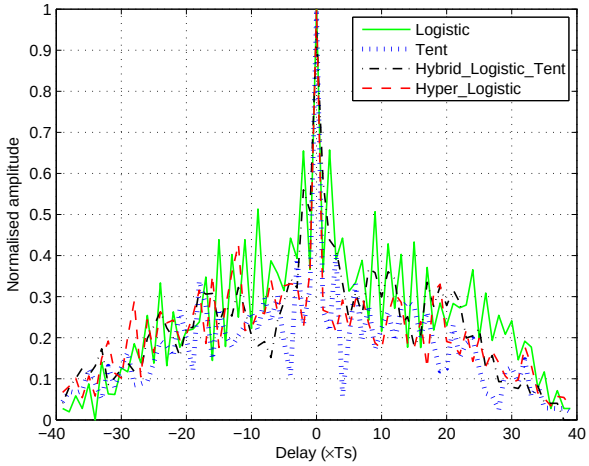

Fig. 3: The synthetic outputs of four different kinds of primary chaotic phase-coded waveforms

B. Verifying the Properties of the STCC

The ACS algorithm is utilized to optimize a pair of complementary chaotic phase-coded sequences. The parameters

TABLE I: PARAMETER SETUP FOR THE ACS

Symbol	Quantity	Value
N_p	population size	10
N	total generation	100
ζ	population diversity	0.002
n_c	clonal size	40
$p_{\max}$	maximum mutation rate	0.7
$p_{\min}$	minimum mutation rate	0.05
μ	weight coefficient	1

This article has been accepted for publication in a future issue of this journal, but has not been fully edited. Content may change prior to final publication. Citation information: DOI 10.1109/ACCESS.2018.2859404, IEEE Access

are set in Table I. The cost function values of $E_{um}(\boldsymbol{b}_m)$ changed with the increase of the generation number are shown in Fig. 4. It is found that the cost values are dramatically decreased at first and gradually decreased with the increase of the evolution generation. This phenomenon agrees well with the adaptive optimization process in the ACS, in which the mutation probability is high at younger generation, and the mutation probability is reduced adaptively with the increase of the generation number. Moreover, we note that under the same optimization condition, better results are obtained for the ACS algorithm with better initial values.

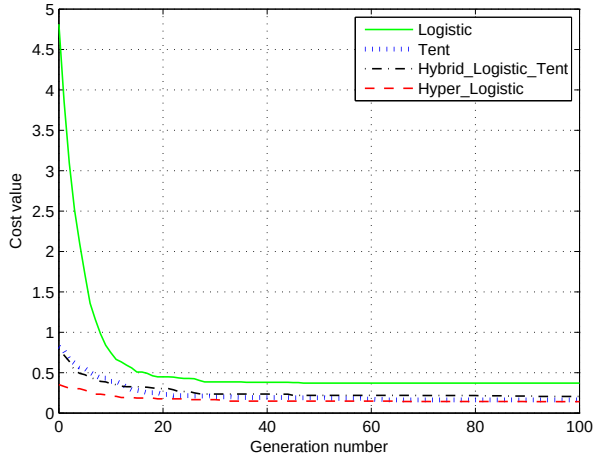

Fig. 4: Cost function values with the increase of the evolution generation

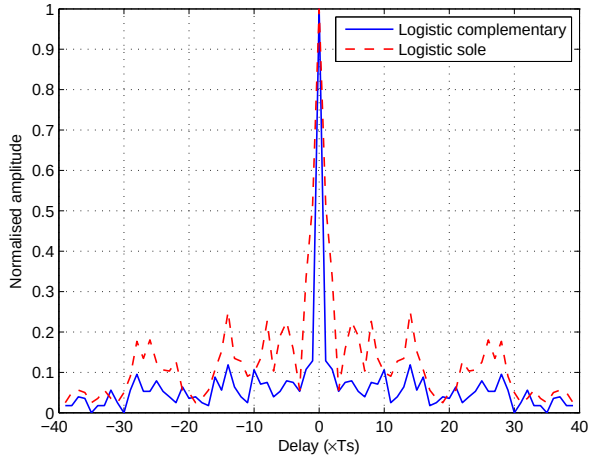

Fig. 5: The autocorrelation properties of sole and complementary chaotic phase-coded waveforms

The complementary property of the optimized sequences is demonstrated in Fig. 5. The sum of the autocorrelation functions of an optimized complementary pair of logistic phase-coded waveforms is presented, and the autocorrelation function of a single logistic phase-coded waveform is also shown. By comparing the sidelobe level of the sole logistic phase-coded waveform with that of the complementary logistic phase-coded waveforms, it is found that the sidelobes are significantly reduced by the complementary optimization. In addition, the mainlobe width of the complementary logistic phase-coded waveforms is narrower than that of the sole logistic phase-coded waveform. Thus, it can be concluded that the optimized complementary phase-coded waveforms can obtain a superior autocorrelation property. Here only the logistic sequences are exemplified for convenience. Other kinds of chaotic sequences have similar results, and the degree of improvement for a better chaotic map is larger.

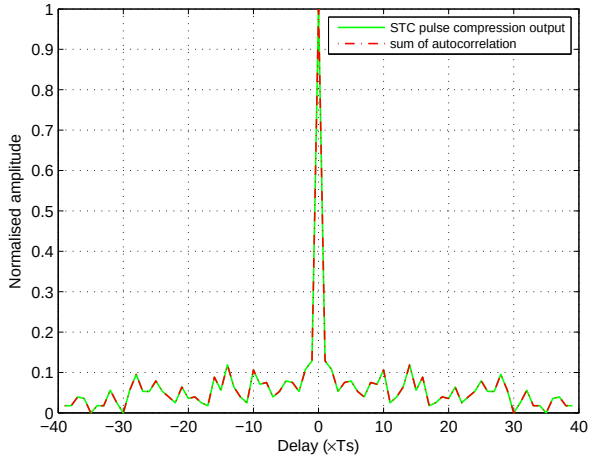

Fig. 6: The effect of STC on complementary waveforms

When the STC is utilized for the optimized complementary chaotic phase-coded waveforms, the crosscorrelation between different transmitted waveforms is eliminated. The synthetic output of the optimized logistic phase-coded waveforms with STCC is compared with the sum of the autocorrelation functions of a complementary pair of logistic phase-coded waveforms, which is shown in Fig. 6. Obviously, the two outputs coincide with each other exactly, which validates the effectiveness of the STCC.

C. Validating the Superiority of the Optimized Chaotic Phase-Coded Waveforms with STCC

Four sets of transmitted waveforms are investigated in this section, which are orthogonal phase-coded waveforms respectively based on four independent chaotic sequences, four independent complementary chaotic sequences, four Deng' codes, and chaotic sequences with STCC. The orthogonal waveform set composed of four complementary pairs of chaotic phase-coded waveforms is generated by repeating the ACS optimization algorithm four times independently. The synthetic outputs $R_r(\boldsymbol{S})$ of those four waveform sets using logistic, tent, hybrid logistic-tent, and hyper logistic maps are shown in Fig. 7(a)-(d), from which we have the following conclusions: (1) The sidelobe level of the four complementary chaotic phase-coded waveforms is much lower than that of those four sole chaotic phase-coded waveforms, and a lit bit lower than that of the Deng's phase-coded waveforms. Also the mainlobe width of the complementary chaotic waveforms

This article has been accepted for publication in a future issue of this journal, but has not been fully edited. Content may change prior to final publication. Citation information: DOI 10.1109/ACCESS.2018.2859404, IEEE Access

is narrower than that of the sole chaotic waveforms, and almost the same with that of the Deng's waveforms. (2) Comparing with Fig. 5, it can be seen that the synthetic outputs of four complementary chaotic phase-coded waveforms and four chaotic phase-coded waveforms are worse than that of the single complementary chaotic phase-coded waveform and the single chaotic phase-coded waveform respectively due to the mutual interferences introduced by other transmitted waveforms. (3) When the STCC is implemented, the synthetic output of the chaotic phase-coded waveforms is significantly improved, which means that lower sidelobes and narrower mainlobe width are obtained. (4) The chaotic phase-coded waveforms with STCC have the optimal correlation properties, and thus have the best synthetic output compared with other three waveform sets. (5) No matter for good chaotic maps or bad chaotic maps, our proposed designing method can enhance their applicability as phase-coded waveforms in MIMO radars.

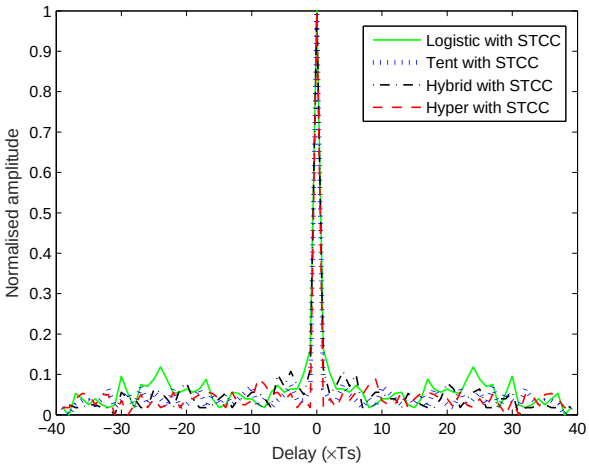

Fig. 8: The synthetic outputs of four different kinds of chaotic phase-coded waveforms with STCC

The synthetic outputs of those four sets of chaotic phase-coded waveforms with STCC using logistic, tent, hybrid logistic-tent, and hyper logistic maps are also demonstrated in Fig. 8. All of them have low sidelobes and narrow mainlobe width. Similar to the synthetic outputs of those four sets of primary chaotic phase-coded waveforms in Fig. 3, it is found that the chaotic sequences with better primary correlation properties have better optimized results with STCC. For instance, the hyper logistic and tent phase-coded waveforms with STCC have relatively the best synthetic outputs, and the logistic phase-coded waveforms with STCC have almost the worst synthetic outputs. However, the difference is small

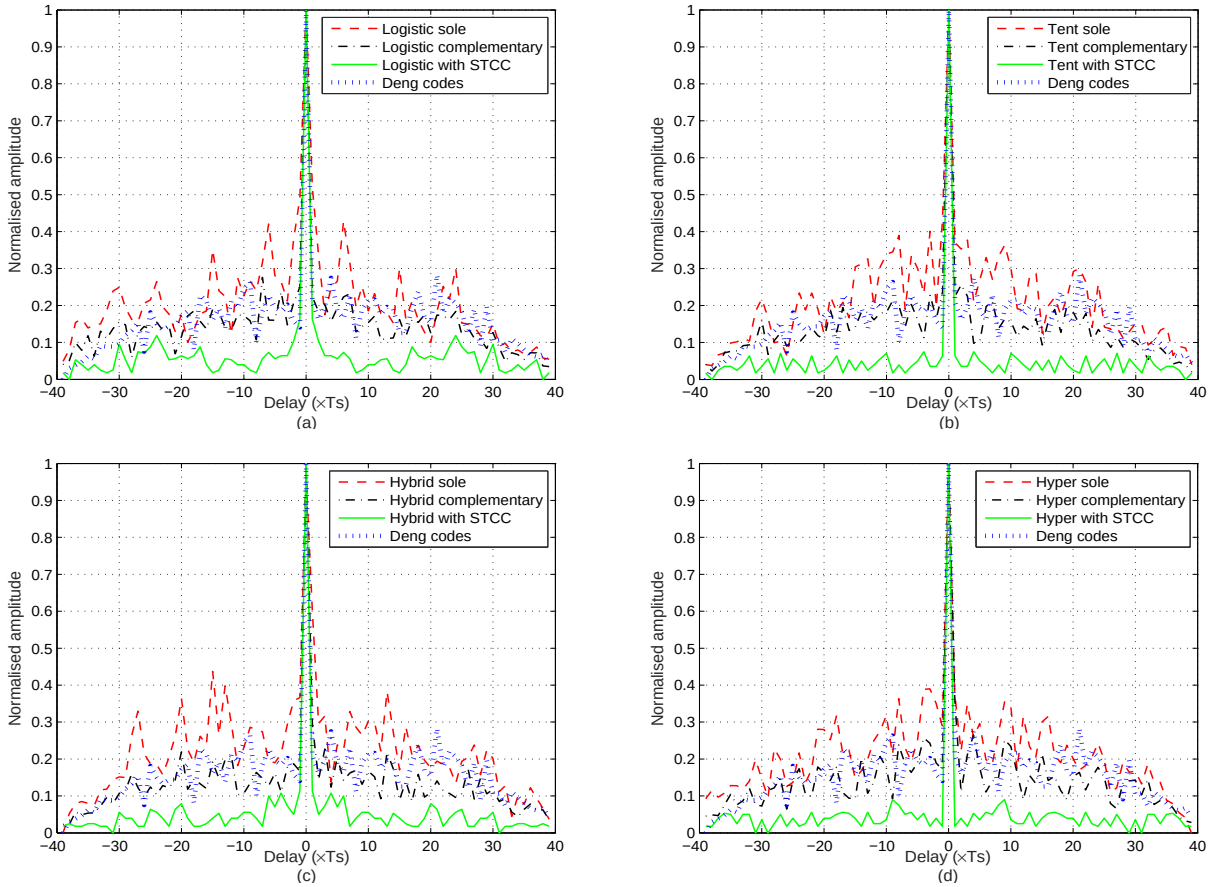

Fig. 7: The synthetic outputs with mutual interferences of different kinds of waveform sets. (a) Logistic based and Deng's; (b) Tent based and Deng's; (c) Hybrid logistic-tent based and Deng's; (d) Hyper logistic based and Deng's.

This article has been accepted for publication in a future issue of this journal, but has not been fully edited. Content may change prior to final publication. Citation information: DOI 10.1109/ACCESS.2018.2859404, IEEE Access

since their performances are all greatly enhanced. The above-mentioned four kinds of chaotic maps are taken as examples to demonstrate that any chaotic map can be utilized in our waveform designing framework, and that better chaotic maps can obtain better optimized waveforms.

D. Doppler Compensation

According to the analysis in Sec.II.D, the Doppler frequency induces a phase shift within the uncompressed coded pulse as $\theta = 2\pi f_d T_r$. When the Doppler phase shift θ is zero, the PSL and ISL of the synthetic output for the chaotic phase-coded waveforms with STCC are low (i.e., $\mathrm{PSL}(0) \approx 0$ and $\mathrm{ISL}(0) \approx 0$), which is conductive for the target detection. When the Doppler phase shift increases, the PSL and ISL for the waveforms gradually increase, which masks other possible targets near the main peak. The synthetic outputs $R_r(\boldsymbol{S}, f_d)$ of the logistic phase-coded waveforms with STCC for $\theta = 0°$, $\theta = 90°$, and $\theta = 130°$ are shown in Fig. 9. Significant degradation in the sidelobe level is observed for large Doppler phase shifts compared with the sidelobe level for zero Doppler phase shift. To mitigate the Doppler effect, the weighting method by a null space vector is applied. The compensated results $R_{rc}(\boldsymbol{S}, f_d)$ are also shown in Fig. 9, which demonstrate that after Doppler compensation, the raised PSL and ISL due to the Doppler phase shift are reduced to be near the level of zero Doppler phase shift.

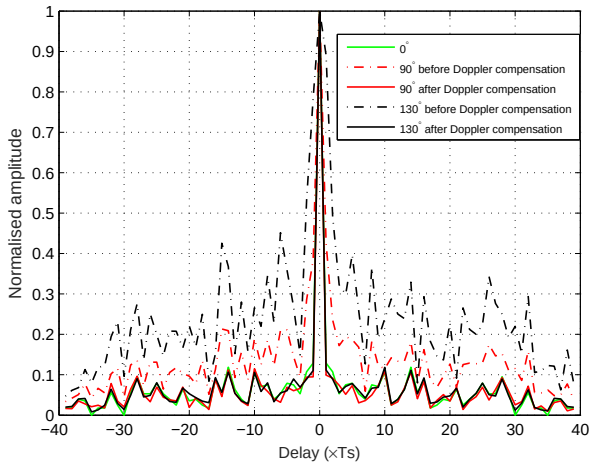

Fig. 9: The synthetic outputs before and after compensation

To comprehensively demonstrate the Doppler intolerance of the waveforms, the synthetic outputs $R_r(\boldsymbol{S}, f_d)$ of the logistic phase-coded waveforms with STCC at different Doppler phase shifts are plotted in Fig. 10, which is equivalent to the MIMO-AF $\chi(\tau, f_d)$ of the designed logistic waveforms. From Fig. 10, it is found that when the Doppler phase shift increases, the synthetic output of the transmitted phase-coded waveforms deteriorates in three aspects: (1) the peak of the mainlobe is dropped. (2) the PSL and ISL of the synthetic output are increased. (3) the mainlobe width is broadened. These phenomena show that the designed waveforms are Doppler-intolerant.

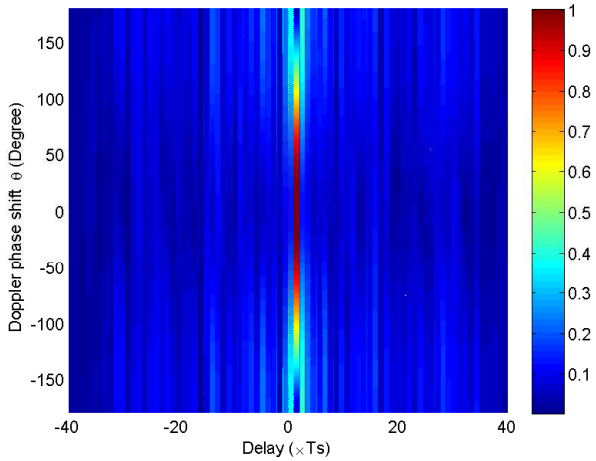

Fig. 10: The synthetic outputs at different Doppler phase shifts

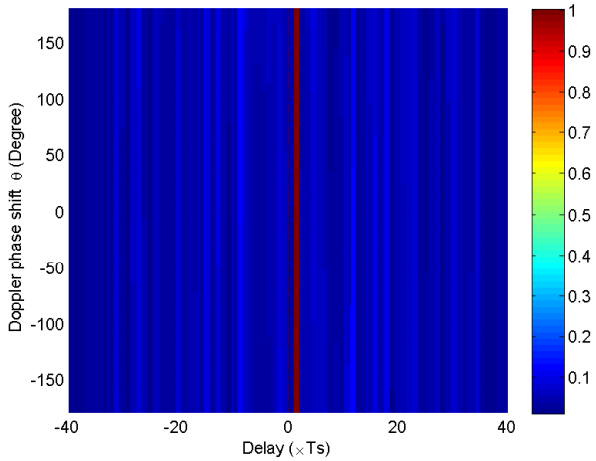

Fig. 11: The compensated synthetic outputs at different Doppler phase shifts

When the received signal is compensated by the weighting method, the compensated synthetic outputs $R_{rc}(\boldsymbol{S}, k, f_d)$ of the logistic phase-coded waveforms with STCC at different Doppler phase shifts are shown in Fig. 11. Obviously, the compensated synthetic output at nonzero Doppler phase shift is almost the same as the synthetic output at zero Doppler phase shift. The effectiveness of the STCC is achieved even for the nonzero Doppler frequency. Thus the sidelobe levels of the synthetic outputs at different Doppler phase shifts are low due to the STCC property and Doppler compensation. The detection ability is enhanced for both the stationary targets and moving targets.

To further verify the effectiveness of the Doppler compensation method in the coherent accumulation process, the PSLs and ISLs of the synthetic outputs with increasing Doppler phase shifts are figured out for different chaotic maps, which are shown in Fig. 12. It can be seen that the sole chaotic phase-coded waveforms, the complementary chaotic phase-coded waveforms, chaotic phase-coded waveforms with STCC, and Deng's phase-coded waveforms are Doppler intolerant, which

This article has been accepted for publication in a future issue of this journal, but has not been fully edited. Content may change prior to final publication. Citation information: DOI 10.1109/ACCESS.2018.2859404, IEEE Access

means that the PSLs and ISLs increase with the absolute Doppler phase shift. Relatively, the proposed transmitted waveforms (chaotic phase-coded waveforms with STCC after Doppler compensation) have lower PSL and ISL, as well as smoother changing trend with increased Doppler phase shifts. It indicates that the proposed transmitted waveforms are much superior in terms of the range sidelobe suppression of pulse compression and Doppler intolerance. With the compensation method, the Doppler tolerance of the proposed waveforms is obtained even for 180° phase shifts as shown in Fig. 12, i.e., $\mathrm{PSL}(f_d) \approx \mathrm{PSL}(0)$ and $\mathrm{ISL}(f_d) \approx \mathrm{ISL}(0)$ for $\forall f_d$ satisfying $|2\pi f_d T_r| \leq 180^\circ$.

It is also noted that compared with the sole chaotic phase-coded waveforms and Deng's phase-coded waveforms, the complementary chaotic phase-coded waveforms and the chaotic phase-coded waveforms with STCC are more sensitive to the Doppler phase shift. However, after the Doppler compensation, the proposed chaotic phase-coded waveforms are almost insensitive to the Doppler phase shift. Compared with Deng's codes, the proposed waveforms after compensation present great improvement in PSL and ISL, whereas compared with solely-transmitted chaotic codes, significant improvements in PSL and ISL are obtained.

From these simulation results, we thus can conclude that the proposed chaotic phase-coded waveforms are much superior to Deng's phase-coded waveforms and sole primary chaotic phase-coded waveforms. Both the sidelobe suppression and Doppler tolerance are achieved.

V. Conclusions

In this paper, a set of chaotic phase-coded waveforms with space-time complementary coding was designed for MIMO radar applications. An adaptive clonal selection algorithm was proposed to optimize independent pairs of complementary chaotic phase-coded waveforms, which can generate a set of quasi-orthogonal waveforms with good autocorrelation properties. To further eliminate the mutual interference of different waveforms, the space-time coding was implemented on the complementary pair. Then a set of ideally orthogonal waveforms with quasi-ideal autocorrelation properties was obtained. The resultant design was a pulse train of phase-coded waveforms, and a Doppler compensation method at the receiver was utilized for the waveforms. In the designing process, three classic problems of autocorrelation, crosscorrelation, and Doppler intolerance were jointly solved, which makes the resultant waveforms extensively usable in practical detection scenarios of MIMO radars. Furthermore, the chaotic systems can provide our optimization a high cardinality set of sequences, and different kinds of chaotic maps can be utilized in our designing methodology. The waveform parameters such

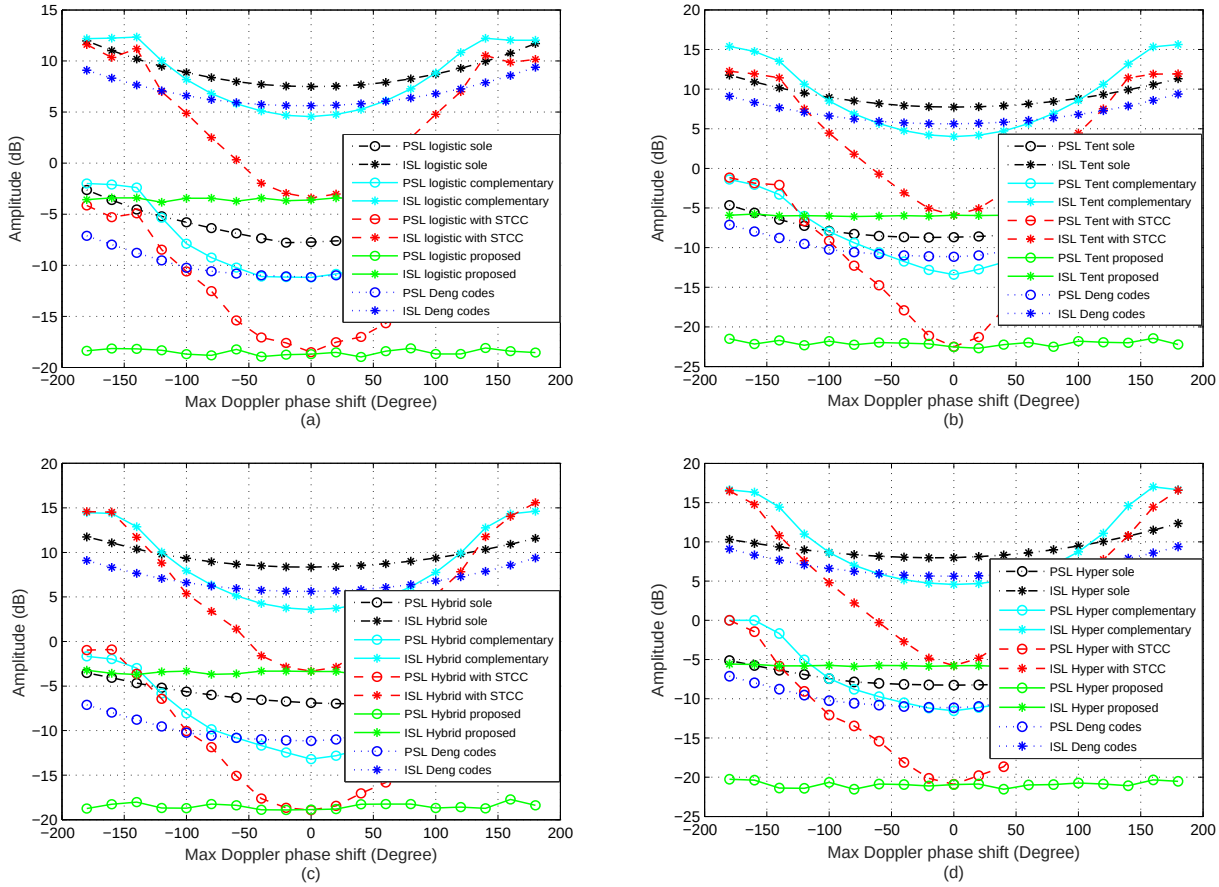

Fig. 12: The PSLs and ISLs of the synthetic outputs of different waveforms with various Doppler phase shifts. (a) Logistic based and Deng's; (b) Tent based and Deng's; (c) Hybrid logistic-tent based and Deng's; (d) Hyper logistic based and Deng's.

This article has been accepted for publication in a future issue of this journal, but has not been fully edited. Content may change prior to final publication. Citation information: DOI 10.1109/ACCESS.2018.2859404, IEEE Access

as the code number, code length, and phase number can also be chosen more freely. Thus the designing methodology offers the waveform generation great flexibility. Simulation results further demonstrated that compared with other waveforms, the matched filtering output of the proposed waveforms has much lower sidelobe level and is almost insensitive to the Doppler phase shift. It indicates that the proposed waveform set is a superior waveform set suitable for MIMO radar applications.

APPENDIX A
THE DERIVATION OF $\chi_{s_m}(\tau, f_d)$

According to the definition of the auto-AF, one has

$$\begin{aligned}\chi_{s_m}(\tau, f_d) &= \int_{-\infty}^{+\infty} s_m(t)s_m^*(t+\tau)\exp(j2\pi f_d t)dt \\ &= \int_{-\infty}^{+\infty}[A_m(t)+B_m(t-T_r)][A_m(t+\tau)+B_m(t+\tau-T_r)]^* \\ &\quad \exp(j2\pi f_d t)dt\end{aligned}. \tag{63}$$

Usually, the considered delay τ satisfies $\tau \in [-T_r, T_r]$. Then (63) can be simplified as

$$\begin{aligned}\chi_{s_m}(\tau, f_d) &= \int_{-\infty}^{+\infty}[A_m(t)A_m^*(t+\tau)\exp(j2\pi f_d t)]dt \\ &+ \int_{-\infty}^{+\infty}[B_m(t-T_r)B_m^*(t+\tau-T_r)\exp(j2\pi f_d t)]dt.\end{aligned} \tag{64}$$

By assuming that $t' = t - T_r$, one has

$$\begin{aligned}&\int_{-\infty}^{+\infty}[B_m(t-T_r)B_m^*(t+\tau-T_r)\exp(j2\pi f_d t)]dt = \\ &\exp(j2\pi f_d T_r)\int_{-\infty}^{+\infty}[B_m(t')B_m^*(t'+\tau)\exp(j2\pi f_d t')]dt'.\end{aligned} \tag{65}$$

By substituting (65) into (64), one has

$$\begin{aligned}\chi_{s_m}(\tau, f_d) &= \int_{-\infty}^{+\infty}[A_m(t)A_m^*(t+\tau)\exp(j2\pi f_d t)]dt \\ &+ \exp(j2\pi f_d T_r)\int_{-\infty}^{+\infty}[B_m(t)B_m^*(t+\tau)\exp(j2\pi f_d t)]dt \\ &= \chi_{A_m}(\tau, f_d) + \exp(j2\pi f_d T_r)\,\chi_{B_m}(\tau, f_d).\end{aligned} \tag{66}$$

The detail derivation for $\chi_{A_m}(\tau, f_d)$ is presented, and the deriving process for $\chi_{B_m}(\tau, f_d)$ is similar to that for $\chi_{A_m}(\tau, f_d)$. The signal $A_m(t)$ defined in (2) can be rewritten as

$$\begin{aligned}A_m(t) &= \sum_{l=0}^{L-1}\exp(ja_m(l))u(t-lT_s) \\ &= u(t) \otimes \sum_{l=0}^{L-1}\exp(ja_m(l))\delta(t-lT_s) \\ &\triangleq u(t) \otimes a_m(t)\end{aligned} \tag{67}$$

where $\otimes$ denotes the convolution operation. $a_m(t)$ is the signal of the phase-coded sequence, and its ambiguity function is denoted by $\chi_{a_m}(\tau, f_d)$. $u(t)$ is the symbol modulation signal, and its ambiguity function is denoted by $\chi_u(\tau, f_d)$. According to the ambiguity function for phase-coded signal [51], $\chi_{A_m}(\tau, f_d)$ can be written as

$$\chi_{A_m}(\tau, f_d) = \chi_{a_m}(\tau, f_d) \underset{\tau}{\otimes} \chi_u(\tau, f_d) \tag{68}$$

$$\chi_{a_m}(iT_s, f_d) = \sum_{l=0}^{L-|i|-1} [\exp(ja_m(l))][\exp(ja_m(l+|i|))]^* \exp(j2\pi f_d l T_s) \tag{69}$$

$$\chi_u(\tau, f_d) = \begin{cases}\frac{\exp(j\pi f_d(T_s-\tau))\sin(\pi f_d(T_s-|\tau|))}{\pi f_d(T_s-|\tau|)}\left(1-\frac{|\tau|}{T_s}\right), & |\tau| \le T_s \\ 0, & |\tau| > T_s\end{cases}. \tag{70}$$

By substituting (69) and (70) into (68), one has

$$\chi_{A_m}(\tau, f_d) = \sum_{i=-(L-1)}^{L-1}\chi_u(\tau - iT_s, f_d)\chi_{a_m}(iT_s, f_d). \tag{71}$$

If $\tau = kT_s$, one has

$$\chi_{A_m}(kT_s, f_d) = \chi_u(0, f_d)\chi_{a_m}(kT_s, f_d) \tag{72}$$

$$\chi_u(0, f_d) = \frac{\exp(j\pi f_d T_s)\sin(\pi f_d T_s)}{\pi f_d T_s}. \tag{73}$$

Similarly, one has

$$\chi_{B_m}(\tau, f_d) = \sum_{i=-(L-1)}^{L-1}\chi_u(\tau - iT_s, f_d)\chi_{b_m}(iT_s, f_d) \tag{74}$$

$$\chi_{B_m}(kT_s, f_d) = \chi_u(0, f_d)\chi_{b_m}(kT_s, f_d) \tag{75}$$

where the $\chi_{b_m}(kT_s, f_d)$ can be directly obtained by replacing the phase code sequence $\boldsymbol{a}_m$ in (69) by $\boldsymbol{b}_m$. By substituting (72) and (74) into (66), the auto-AF $\chi_{s_m}(kT_s, f_d)$ is obtained as

$$\begin{aligned}\chi_{s_m}(kT_s, f_d) =& \chi_u(0, f_d)[\chi_{a_m}(kT_s, f_d) \\ &+ \exp(j2\pi f_d T_r)\chi_{b_m}(kT_s, f_d)].\end{aligned} \tag{76}$$

APPENDIX B
THE DERIVATION OF $\chi_{s_m,s_n}(\tau, f_d)$

According to the definition of the cross-AF, one has

$$\begin{aligned}\chi_{s_m,s_n}(\tau, f_d) &= \int_{-\infty}^{+\infty} s_m(t)s_n^*(t+\tau)\exp(j2\pi f_d t)dt \\ &= \int_{-\infty}^{+\infty}[A_m(t)+B_m(t-T_r)][A_n(t+\tau)+B_n(t+\tau-T_r)]^* \\ &\quad \exp(j2\pi f_d t)dt\end{aligned}. \tag{77}$$

Using the similar manipulations for (64) and (65), one has

$$\begin{aligned}\chi_{s_m,s_n}(\tau, f_d) &= \int_{-\infty}^{+\infty}[A_m(t)A_n^*(t+\tau)\exp(j2\pi f_d t)]dt \\ &+ \exp(j2\pi f_d T_r)\int_{-\infty}^{+\infty}[B_m(t)B_n^*(t+\tau)\exp(j2\pi f_d t)]dt \\ &= \chi_{A_m,A_n}(\tau, f_d) + \exp(j2\pi f_d T_r)\,\chi_{B_m,B_n}(\tau, f_d).\end{aligned} \tag{78}$$

By referring to the derivation for $\chi_{A_m}(\tau, f_d)$, the $\chi_{A_m,A_n}(\tau, f_d)$ can be written as

$$\chi_{A_m,A_n}(\tau, f_d) = \sum_{i=-(L-1)}^{L+1} \chi_u(\tau - iT_s, f_d)\chi_{a_m,a_n}(iT_s, f_d) \tag{79}$$

$$\chi_{a_m,a_n}(iT_s, f_d) = \sum_{l=0}^{L-|i|-1} \frac{[\exp(ja_n(l))][\exp(ja_m(l+|i|))]^*}{\exp(j2\pi f_d l T_s)}. \tag{80}$$

If $\tau = kT_s$, one has

$$\chi_{A_m,A_n}(kT_s, f_d) = \chi_u(0, f_d)\chi_{a_m,a_n}(kT_s, f_d). \tag{81}$$

Similarly, one has

$$\chi_{B_m,B_n}(\tau, f_d) = \sum_{i=-(L-1)}^{L+1} \chi_u(\tau - iT_s, f_d)\chi_{b_m,b_n}(iT_s, f_d) \tag{82}$$

$$\chi_{B_m,B_n}(kT_s, f_d) = \chi_u(0, f_d)\chi_{b_m,b_n}(kT_s, f_d) \tag{83}$$

where the $\chi_{b_m,b_n}(kT_s, f_d)$ can be directly obtained by replacing the phase code sequence $\boldsymbol{a}_m$ in (80) by $\boldsymbol{b}_m$. By substituting (81) and (83) into (78), the cross-AF $\chi_{s_m,s_n}(kT_s, f_d)$ is obtained as

$$\begin{aligned}\chi_{s_m,s_n}(kT_s, f_d) =& \chi_u(0, f_d)[\chi_{a_m,a_n}(kT_s, f_d) \\ &+ \exp(j2\pi f_d T_r)\chi_{b_m,b_n}(kT_s, f_d)].\end{aligned} \tag{84}$$

REFERENCES

[1] J. Li and P. Stoica, MIMO Radar Signal Processing, Hoboken, NJ, USA: Wiley, 2009.

[2] S. B. Yuan, S. Jin, and T. L. Zhu, "The development review of MIMO radar technology," *Modern Radar*, vol. 39, no. 8, pp. 5-8, 2017.

[3] Z. Liu, X. Zhu, W. Hu, and F. Jiang, "Principles of chaotic signal radar," *Int. J. Bifurcation Chaos*, vol. 17, no. 5, pp. 1735-1739, 2007.

[4] M. S. Willsey, K. M. Cuomo, and A. V. Oppenheim, "Quasi-orthogonal wideband radar waveforms based on chaotic systems," *IEEE Trans. Aerosp. Electron. Syst*, vol. 47, no. 3, pp. 1974-1984, Jul. 2011.

[5] H. E. Najafabadi, M. Ataei, and M. F. Sabahi, "Chebyshev chaotic polynomials for MIMO radar waveform generation," *IET Radar, Sonar & Navigation*, vol. 11, no. 2, pp. 330-340, Feb. 2017.

[6] E. N. Hamid, M. Ataei, and M. F. Sabahi, "Designing sequence with minimum PSL using Chebyshev distance and its application for chaotic MIMO radar waveform design," *IEEE Trans. Signal Process.*, vol. 65, no. 3, pp. 90-704, Feb. 2017.

[7] B. J. Zouhair and B. Safya, "Chaotic sequences with good correlation properties for MIMO Radar application," *the 24th International Conference on Software, Telecommunications and Computer Networks (SoftCOM)*, Split, Croatia, Sep. 2016.

[8] Q. D. Huang, Y. Li, Y. P. Zeng, and Y. J. Fu, "Design and characteristic analysis of multicarrier chaotic phase coded radar pulse train signal," *Int. J. Antenn. Propag.*, pp. 1-8, 2014.

[9] B. S. Liu and W. L. Zhang, "Design of chaotic orthogonal discrete frequency coding waveform," *International Conference on Education, Management and Computer Science (ICEMC)*, Shenyang, Peoples R China, May. 2016.

[10] Y. Zhu, S. Hadjiloucas, J. Chen, and W. Long, "The chaotic frequency hopping signals for MIMO radar," *Journal of Computational Information Systems*, vol. 10, no. 10, pp. 4261-4269, 2014.

[11] T. F. Yao, D. Zhu, D. Ben, and S. L. Pan, "Distributed MIMO chaotic radar based on wavelength-division multiplexing technology," *Opt. Lett.*, vol. 40, no. 8, Apr. 2015.

[12] R. M. Davis, R. L. Fante, and R. P. Perry, "Phase-coded waveforms for radar," *IEEE Trans. Aerosp. Electron. Syst*, vol. 43, no. 1, April. 2007.

[13] X. Feng, Z. K. Chen, Y. N. Zhao, and F. C. Li, "Phase-coded waveform design via relaxed alternating projection for MIMO radar," *Acta Electronica Sinica*, vol. 44, no. 12, pp. 2981-2988, 2016.

[14] X. Wu, W. Liu, and L. Zhao, "Chaotic phase code for radar pulse compression," *in Proc. IEEE 2001 Radar Conference*, Atlanta, GA, May. 2001, pp. 279-283.

[15] H. Deng,"Poly-phase code design for orthogonal netted radar system," *IEEE Trans. Signal Process.*, vol. 52, no. 11, pp. 3126-3135, 2004.

[16] H. A. Khan, Y. Y. Zhang, C. L. Ji, C. J. Stevens, D. J. Edwards, and D. O'Brien, "Optimizing polyphase sequences for orthogonal netted radar," *IEEE Signal Process. Lett.*, vol. 13, pp. 589-592, 2006.

[17] H. P. Hu and B. Liu, "Genetic algorithm for designing polyphase orthogonal code," *Wireless Communications, Networking and Mobile Computing*, pp. 1-4, 2008.

[18] Z. Dunn, M. Yeary, F. Uysal, and C. Fulton, "Low sidelobe pseudo-orthogonal code sets through particle swarm optimization," *IEEE 2016 Radar Conference*, Philadelphia, USA, Jun. 2016, pp. 194-197.

[19] G. L. Cui, X. X. Yu, M. Piezzo, and L. J. Kong, "Constant modulus sequence set design with good correlation properties," *Signal Process.*, vol. 139, pp. 75-85, Oct. 2017.

[20] H. A. Khan and D. J. Edwards, "Doppler problems in orthogonal MIMO radars," *IEEE Conf. Radar*, Verona, USA, Apr. 2006, pp. 244-247.

[21] N. Levanon and E. Mozeson, Radar Signals, Hoboken, NJ, USA: Wiley, 2004.

[22] M. A. Kerahroodi, A. AubryA, A. De MaioD, and M. M. Naghsh, "A coordinate-descent framework to design low PSL/ISL sequences," *IEEE Trans. Signal Process.*, vol. 65, no. 22, pp. 5942-5956, Nov. 2017.

[23] R. L. Frank, "Polyphase codes with good nonperiodic correlation properties," *IEEE Trans. Inf. Theory*, vol. IT-9, no. 1, pp. 43-45, Jan. 1963.

[24] M. Golay, "Complementary series," *IEEE Trans. Inf. Theory*, vol. IT-7, no. 2, pp. 82-87, Apr. 1961.

[25] J. X. Song, P. Babu and D. P. Palomar, "Sequence set design with good correlation properties via majorization-minimization," *IEEE Trans. Signal Process.*, vol. 64, no. 11, pp. 2866-2879, Jun. 2016.

[26] G. J. Frazer, Y. I. Abramovich, and B. A. Johnson. "Recent results in MIMO over-the-horizon radar," *in IEEE Radar Conference, RADAR'08*, Rome, Italy, May. 2008, pp. 1-6.

[27] Z. Niu, B. Pei, J. Chen, and X. Gao, "Study on design of orthogonal signal for MIMO over-the-horizon radar," *Video Engineering*, vol. 36, no. 1, pp. 98-100, 2012.

[28] X. F. Song, S. L. Zhou, and P. Willett, "Reducing the waveform cross correlation of MIMO radar with space time coding," *IEEE Trans. Signal Process.*, vol. 58, no. 8, pp. 4213-4224, Oct. 2008.

[29] L. Lo Monte, T. A. Corigliano, and B. Himed, "Dynamic range considerations in code division multiple input multiple output radar," *IET Radar Sonar & Navigation*, vol. 10, no. 8, pp. 1375-1383, Oct. 2016.

[30] S. H. Zhou, H. W. Liu, and H. K. Zang, "Doppler sensitivity of MIMO radar waveforms," *IEEE Trans. Aerosp. Electron. Syst*, vol. 52, no. 5, pp. 2091-2110, Oct. 2016.

[31] M. M. Chitgarha, M. Radmard, M. N. Majd, S. M. Karbasi, and M. M. Nayebi, "MIMO radar signal design to improve the MIMO ambiguity function via maximizing its peak," *Signal Process.*, vol. 118, pp. 139-152, Jan. 2016.

[32] X. Feng, Y. N. Zhao, Z. Q. Zhou, and Z. F. Zhao, "Waveform design with low range sidelobe and high Doppler tolerance for cognitive radar," *Signal Process.*, vol. 139, pp. 143-155, Oct. 2017.

[33] H. A. Khan, Y. Zhang, C. Ji, C. J. Stevens, D. J. Edwards, and D. O'Brien, "Optimizing polyphase sequences for orthogonal netted radar," *IEEE Signal Process. Lett.*, vol. 13, no. 10, pp. 589-592, Oct. 2006.

[34] H. D. Nguyen and G. E. Coxson, "Doppler tolerance, complementary code sets, and generalised Thue-Morse sequences," *IET Radar, Sonar & Navigation*, vol. 10, no. 9, pp. 1603-1610, 2016.

[35] A. Pezeshki, A. R. Calderbank, and W. Moran et al., "Doppler resilient golay complementary waveforms," *IEEE Trans. Inf. Theory*, vol. 54, no. 9, pp. 4254-4266, Sep. 2008.

[36] R. Takahashi, T. Takahashi, and H. Tasaki, "Doppler compensation of MISO range response in subband division LFM pulse MIMO radar," *21st International Symposium on Antennas and Propagation (ISAP)*, Okinawa, Japan, Oct. 2016.

[37] M. Skolnik, Pulse Compression Radar, 2nd ed., New York: McGraw-Hill, 1990, ch. 10.

[38] X. B. Dong, D. X. Zhao, B. Yang, and C. H. Han, "Fractional-order control of active suspension actuator based on parallel adaptive clonal

selection algorithm," *Journal of Mechanical Science and Technology*, vol. 30, no. 6, pp. 2769-2781, Jun. 2016.

[39] S. D. Howard, A. R. Calderbank, and W. Moran, "A simple signal processing architecture for instantaneous radar polarimetry," *IEEE Trans. Inf. Theory*, vol. 53, no. 4, pp. 1282-1289, Apr. 2007.

[40] S. A. Harman, "The diversity of chaotic waveforms in use and characteristics," *2006 IET Seminar on Waveform Diversity and Design in Communications, Radar and Sonar*, London, UK, Nov. 2006, pp. 33-40.

[41] Q. B. Luo and J. Zhang, "Research on spreading sequences with a novel chaos," *System Engineering and Electronics*, vol. 28, no. 10, pp. 1497-1499, Oct. 2006.

[42] Y. K. Deng, Y. H. Hu, and X. P. Geng, "Hyper chaotic logistic phase coded signal and its sidelobe suppression," *IEEE Trans. Aerosp. Electron. Syst*, vol. 46, no. 2, pp. 672-686, April. 2010.

[43] K. Huo and J. J. Zhao, "A design method of four-phase-coded OFDM radar signal based on Bernoulli chaos," *Journal of Radars*, vol. 5, no. 4, pp. 361-372, 2016.

[44] C. Y. Chen and P. P. Vaidyanathan, "MIMO radar ambiguity properties and optimization using frequency-hopping waveforms," *IEEE Trans. signal processing*, vol. 56, no.12, pp. 5926-5936, 2008.

[45] C. C. Tseng and C. L. Liu, "Complementary sets of sequences," *IEEE Trans. Inf. Theory*, vol. IT-18, no. 5, pp. 644-652, Sep. 1972.

[46] R. L. Frank, "Polyphase complementary codes," *IEEE Trans. Inf. Theory*, vol. IT-26, no. 6, pp. 641-647, Nov. 1980.

[47] M.B. Hawes, W. Liu, "Pattern synthesis of linear antenna arrays using a genetic algorithm with physical size constraint," *Proceedings of 6th European Conference on Antennas and Propagation*, Prague, Czech Republic, Jun. 2012, pp. 3046-3049.

[48] A. F. Naguib, T. Vahid, and N. Seshadri, "A space-time coding modem for high-data-rate wireless communications," *IEEE J. Sel. Areas Commun.*, vol. 16, no. 8, pp. 1459-1478, 1998.

[49] Z. Q. Liu, G. B. Giannakis, S. Barbarossa et al., "Transmit-antennae space-time block coding for generalized OFDM in the presence of unknown multipath," *IEEE J. Sel. Areas Commun.*, vol. 19, no. 7, pp. 1352-1364, 2001.

[50] X. L. Du, T. Su, X. Wang, W. T. Zhu, B. Jin, and L. Zhang, "Golay complementary sequence with space time coding for MIMO radar waveform design," *Journal of Electronics & Information Technology*, vol. 36, no. 8, pp. 1967-1971, Aug. 2014.

[51] A. M. Hu and K. X. Hu, "Application of phase-coding signal in radar," *Shipboard Electronic Countermeasure*, vol. 30, no. 5, pp. 66-82, October, 2007.